Inorganic Chemistry

Article

pubs.acs.org/IC

U^{III}–CN versus U^{IV}–NC Coordination in Tris(silylamide) Complexes

Alexandre Hervé,[†] Yamina Bouzidi,[‡] Jean-Claude Berthet,*[,†] Lotfi Belkhiri,*[,‡] Pierre Thuéry,[†] Abdou Boucekkine,*[,§] and Michel Ephritikhine*[,†]

[†]CEA, IRAMIS, UMR 3685 NIMBE, CEA/CNRS NIMBE, CEA/Saclay, 91191 Gif-sur-Yvette, France

[‡]URCHEMS, Département de chimie, Université Constantine 1, 25000 Constantine, Algeria

[§]Institut des Sciences Chimiques de Rennes, UMR 6226 CNRS - Université de Rennes 1, Campus de Beaulieu, 35042 Rennes Cedex, France

Supporting Information

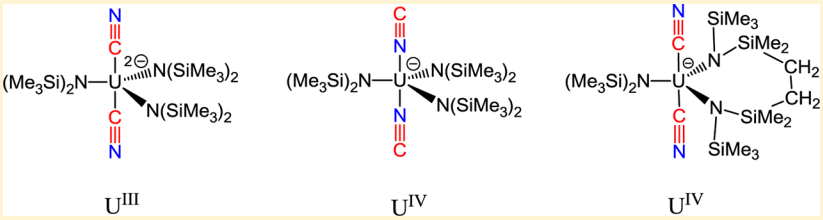

U^{III} U^{IV} U^{IV}

ABSTRACT: Treatment of the metallacycle [UN*$_2$(*N*,*C*)] [N* = N(SiMe$_3$)$_2$; *N*,*C* = CH$_2$SiMe$_2$N(SiMe$_3$)] with [HNEt$_3$][BPh$_4$], [HNEt$_3$]Cl, and [pyH][OTf] (OTf = OSO$_2$CF$_3$) gave the cationic compound [UN*$_3$][BPh$_4$] (**1**) and the neutral complexes [UN*$_3$X] [X = Cl (**3**), OTf (**4**)], respectively. The dinuclear complex [{UN*(*μ*-*N*,*C*)(*μ*-OTf)}$_2$] (**5**) and its tetrahydrofuran (THF) adduct [{UN*(*N*,*C*)(THF)(*μ*-OTf)}$_2$] (**6**) were obtained by thermal decomposition of **4**. The successive addition of NEt$_4$CN or KCN to **1** led to the formation of the cyanido-bridged dinuclear compound [(UN*$_3$)$_2$(*μ*-CN)][BPh$_4$] (**7**) and the mononuclear mono- and bis(cyanide) complexes [UN*$_3$(CN)] (**2**) and [M][UN*$_3$(CN)$_2$] [M = NEt$_4$ (**8**), K(THF)$_4$ (**9**)], while crystals of [K(18-crown-6)][UN*$_3$(CN)$_2$] (**10**) were obtained by the oxidation of [K(18-crown-6)][UN*$_3$(CN)] with pyridine *N*-oxide. The THF adduct of **1**, [UN*$_3$(THF)][BPh$_4$], and complexes **2**–**7**, **9** and **10** were characterized by their X-ray crystal structure. In contrast to their U^{III} analogues [NMe$_4$][UN*$_3$(CN)] and [K(18-crown-6)]$_2$[UN*$_3$(CN)$_2$] in which the CN anions are coordinated to the metal center via the C atom, complexes **2** and **9** exhibit the isocyanide U–NC coordination mode of the cyanide ligand. This U^{III}/U^{IV} differentiation has been analyzed using density functional theory calculations. The observed preferential coordinations are well explained considering the electronic structures of the different species and metal–ligand bonding energies. A comparison of the different quantum descriptors, i.e., bond orders, NPA/QTAIM data, and energy decomposition analysis, has allowed highlighting of the subtle balance between covalent, ionic, and steric factors that govern the U–CN/NC bonding.

INTRODUCTION

Recently, we reported on the series of uranium(III) cyanide complexes [M][(UN*$_3$)$_2$(*μ*-CN)], [M][UN*$_3$(CN)], [M]$_2$[UN*$_3$(CN)$_2$], and [M]$_2$[UN*$_2$(CN)$_3$] [M = K(18-crown-6) or NR$_4$; N* = N(SiMe$_3$)$_2$], which have been synthesized by the addition of NR$_4$CN (R = Me, Et, ^{n}Bu) or KCN in the presence of 18-crown-6 to the tris(silylamide) precursor [UN*$_3$].[1] Structural comparisons of these compounds with the Ce^{III} analogues revealed the distinct coordination modes of the CN group, through the C or N atom to the U or Ce metal center, respectively, and this differentiation was related to the better energy matching between the 6d/5f U and ligand orbitals, leading to a nonnegligible covalent character of the U–CN bond. In order to extend the variety of soluble molecular cyanide complexes of the actinides and lanthanides, in different oxidation states, which could serve as valuable building blocks for the synthesis of novel clusters and coordination polymers with interesting physicochemical properties, we have then prepared the corresponding U^{IV} compounds [UN*$_3$(CN)] (**2**), [(UN*$_3$)$_2$(*μ*-CN)][BPh$_4$] (**7**), and [M][UN*$_3$(CN)$_2$] [M = NEt$_4$ (**8**), K(THF)$_4$ (**9**)], thus extending the series of [UN*$_3$X] derivatives, which constitute one of the most popular families of complexes in uranium chemistry.[2] These compounds could be synthesized either by the oxidation of [UN*$_3$] and the aforementioned uranium(III) cyanide complexes or by the addition of MCN to the novel cationic U^{IV} precursor [UN*$_3$][BPh$_4$] (**1**). However, the main objective of this study was, from solid-state structural comparisons on uranium(III) and uranium(IV) cyanide counterparts, to demonstrate the influence of the electronic configuration, $5f^3$ or $5f^2$, on the ligation mode of the CN ligand. The X-ray crystal structures revealed the preferential coordination of the cyanide ($^-$CN) and isocyanide (CN$^-$) ions in the uranium(III) and uranium(IV) tris-N* complexes, respectively, and this difference was

Received: January 6, 2015
Published: February 16, 2015

DOI: 10.1021/acs.inorgchem.5b00034
Inorg. Chem. 2015, 54, 2474–2490

Scheme 1. Synthesis of the Complexes

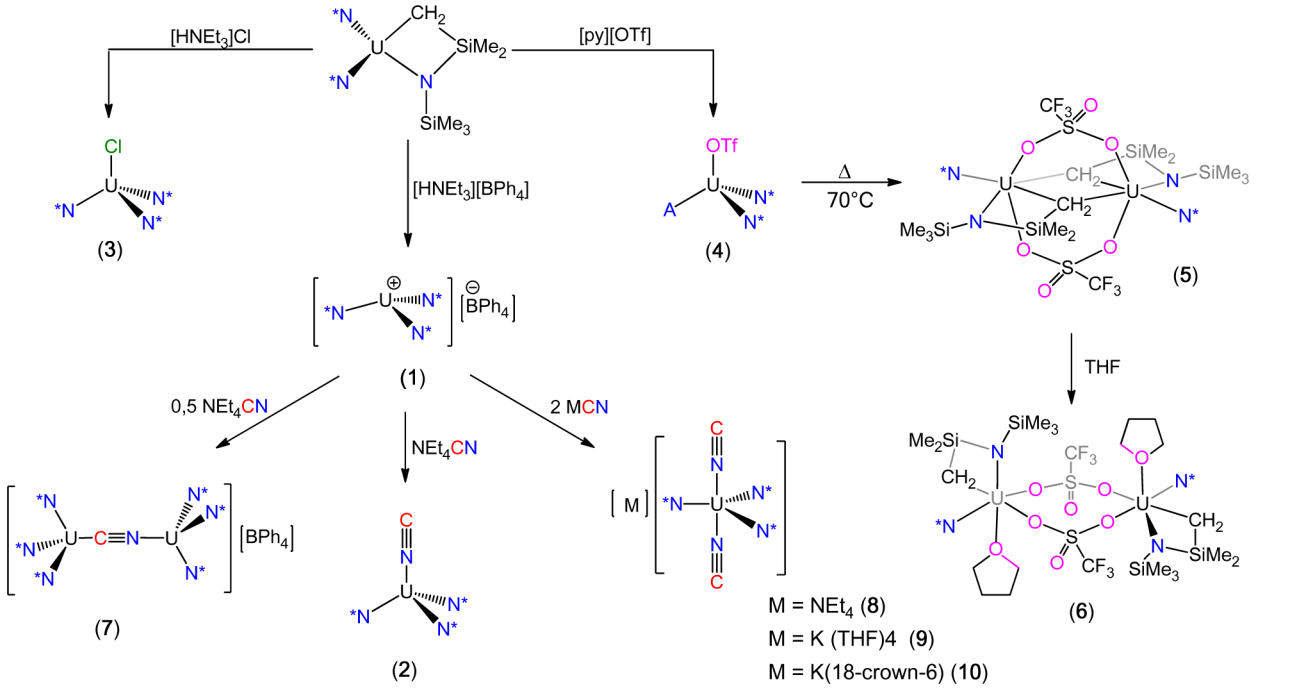

analyzed using relativistic density functional theory (DFT) calculations.

RESULTS AND DISCUSSION

The syntheses of the complexes are summarized in Scheme 1.

[UN*$_3$X] Complexes (X = Cl, OSO$_2$CF$_3$, CN). Taking as an example the reaction of [UN*$_3$] with CuCl, which afforded [UN*$_3$(Cl)] (**3**) in good yield,[3] our first attempts at the preparation of the mono(cyanide) complex **2** consisted of the oxidation of [UN*$_3$] with CuCN. The reaction was performed in benzene and unexpectedly gave the metallacycle [UN*$_2$(*N*,*C*)] [*N*,*C* = CH$_2$SiMe$_2$N(SiMe$_3$)] as the sole uranium compound.[4−6] Using other oxidizing reagents [AgCN, RCN (R = Me, Ph, Me$_3$Si), benzoquinone, Me$_3$NO] and/or [M][UN*$_3$(CN)] [M = NR$_4$ or K(18-crown-6)] as the starting product gave unidentified compounds. In one reaction of [K(18-crown-6)][UN*$_3$(CN)] and pyridine *N*-oxide, pink crystals of the bis(cyanide) complex [K(18-crown-6)][UN*$_3$(CN)$_2$] (**10**) were isolated and characterized by X-ray diffraction analysis (vide infra). The synthesis of **2** from the U^{IV} precursor **3** was then considered, but in contrast to [U(Cp*)$_2$UX$_2$] (Cp* = η-C$_5$Me$_5$; X = I, OSO$_2$CF$_3$), which reacted with KCN or NEt$_4$CN to give [U(Cp*)$_2$(CN)$_2$],[7] **3** did not undergo straightforward substitution with cyanide ligands but was transformed into the addition product [NEt$_4$][UN*$_3$(Cl)(CN)].

These unsuccessful attempts led us to consider the synthesis of **2** by the simple addition of MCN to the cationic precursor **1**, with the easy elimination of the MBPh$_4$ salt. While attempts to prepare in THF the U^{IV} cation [UN*$_3$]$^+$ by one-electron oxidation of [UN*$_3$] led to the rapid catalytic polymerization of the solvent and the formation of [UN*$_4$] in low yield,[8] complex **1** was readily obtained by treating the metallacycle [UN*$_2$(*N*,*C*)] with 1 mol equiv of [HNEt$_3$][BPh$_4$] in THF and, after evaporation of the solvent, isolated as a beige powder in 86% yield. The selectivity of the protonolysis reaction is related to the larger nucleophilic character of the C atom of the *N*,*C* metallacycle, which was already noted in the insertion reactions of small molecules into the U−C bond.[5,9] Importantly, the reaction did not proceed in toluene and the reaction time in THF must be limited (not to exceed 30 min) because of degradation of the cation and the formation of intractable products. Nevertheless, pale-green crystals of the THF adduct [UN*$_3$(THF)][BPh$_4$] [**1**(THF)] were formed by the slow diffusion of diethyl ether (Et$_2$O) into a THF solution of **1**, and this adduct was converted back to **1** upon exposure to a vacuum. The ^{1}H NMR spectrum of **1** in benzene-d_6 shows, in addition to the N* signal integrating for 54 H at δ −6.33, three phenyl resonances in the intensity ratio of 4:8:8 at δ 2.91, 2.82, and 1.60, suggesting that **1** adopts a zwitterionic structure in the solid state or in noncoordinating solvents, with phenyl groups of BPh$_4$ coordinated to the U atom, as previously observed with [U(NEt$_2$)$_3$][BPh$_4$][10] and [U(Cp*)$_2$][BPh$_4$].[11] The treatment of **1** with 0.9 mol equiv of NEt$_4$CN in THF led to formation of the pale-pink powder **2**, which was obtained in 75% yield after extraction in Et$_2$O. Pink crystals of **2** were formed by crystallization from THF.

The metallacycle [UN*$_2$(*N*,*C*)] was also useful for the synthesis of [UN*$_3$X] derivatives, and its protonolysis reactions with 1 mol equiv of [HNEt$_3$]Cl and [pyH][OTf] (OTf = OSO$_2$CF$_3$) gave the chloride and triflate complexes **3** and [UN*$_3$(OTf)] (**4**) in good yield. Complex **4** was also obtained by the oxidation of [UN*$_3$] with Ph$_3$COTf, but it was difficult to separate it from Gomberg's dimer (Ph$_3$CCH(C$_4$H$_4$)C═CPh$_2$), which was formed as a soluble byproduct.[12] The same difficulty was encountered in the synthesis of **3** by the oxidation of [UN*$_3$] with Ph$_3$CCl.[13] The pyridinium triflate was already used for the synthesis of triflate complexes by protonolysis of amide or alkyl precursors and, in particular, [U(OTf)$_4$(py)] was obtained by treating [UN*$_2$(*N*,*C*)] with 4 mol equiv of [pyH][OTf].[14] The chloride **3** was previously synthesized by the reaction of UCl$_4$ with NaN*,[15] the treatment of [UN*$_2$(*N*,*C*)] by HCl,[9] and the oxidation of [UN*$_3$] with CuCl[3] or Ph$_3$CCl,[13] but its crystal structure has not been

DOI: 10.1021/acs.inorgchem.5b00034
Inorg. Chem. 2015, 54, 2474−2490

Scheme 2. Thermal Evolution of Complex 4

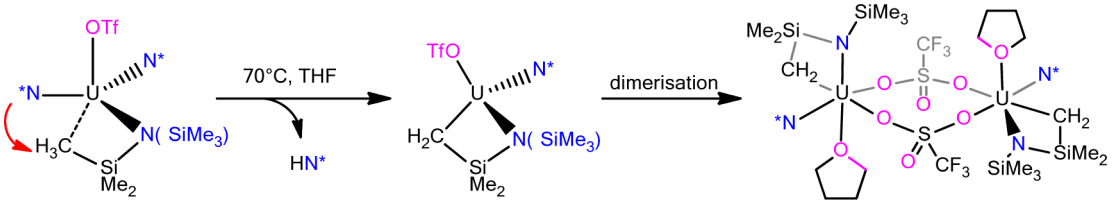

determined. Brown crystals of **3** and pinkish crystals of **4** suitable for X-ray diffraction analysis were formed at −35 °C by crystallization from pentane and a pentane−THF mixture, respectively. Complex **4** was converted in refluxing THF to the metallacycle $[\{UN^*(\mu\text{-}N,C)(\mu\text{-}OTf)\}_2]$ (**5**), isolated as brown crystals in 42% yield after crystallization from Et_2O, and yellow platelets of the THF adduct $[\{UN^*(N,C)(THF)(\mu\text{-}OTf)\}_2]$ (**6**) crystallized from this solvent. The synthesis of **5** could occur via the concerted elimination of HN*, which proceeds under thermal conditions (Scheme 2).[4,8]

The distinct ligation modes of the U(*N*,*C*) metallacycles, bridging in **5** and terminal in **6**, are clearly differentiated by the ^{1}H NMR signals of the methylene groups, which are visible at δ −520.1 and −228.7, respectively.

Views of one of the two independent and very similar cations of **1**(THF) and of the cyanide, chloride, and triflate compounds **2**−**4** are presented in Figures 1−4, respectively, and selected bond lengths and angles are listed in Table 1. The complexes adopt a pseudotetrahedral structure with the exception of the cyanide **2**, which is in a trigonal-pyramidal configuration, with the U1 and N atoms of the N* ligands being almost coplanar, as shown by the sum of the N−U1−N angles equal to 358.5°. The U1 and U2 atoms of the cations $[UN^*_3(THF)]^+$ in **1**(THF), which are at a distance of 0.3843(12) and 0.5250(12) Å from the plane of the three N atoms, exhibit γ U···H−C agostic-type interactions [U1···C1 = 2.892(3) Å and U2···C23 = 3.050(3) Å, with C1 and C23 being in the trans position with respect to the O atom of the THF ligand]. The distance between the metal center and the plane of the amide N atoms in complexes $[UN^*_3X]$ increases with X in the order F [0.1158(9) Å][16] < CN [0.157(4) Å] < Cl [0.406(2) Å] < I

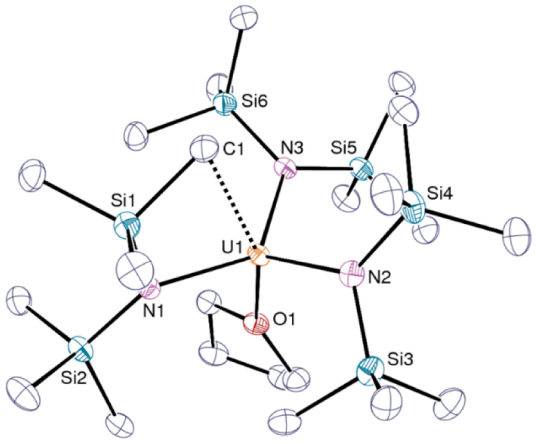

Figure 1. View of one of the two independent cations in **1**(THF). H atoms are omitted. The agostic bond is shown as a dashed line. Displacement ellipsoids are drawn at the 30% probability level.

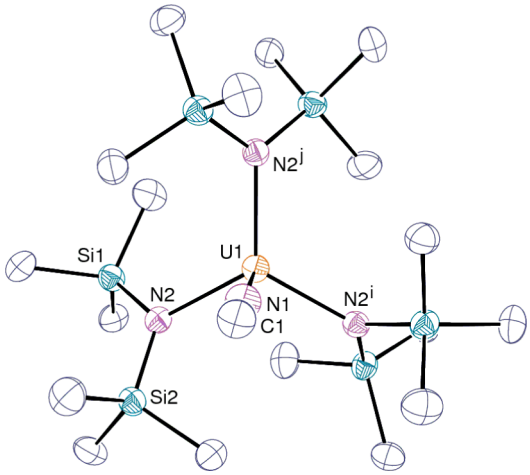

Figure 2. View of complex **2**. H atoms are omitted. Displacement ellipsoids are drawn at the 50% probability level. Symmetry codes: i, 2 − *y*, *x* − *y* + 1, *z*; j, *y* − *x* + 1, 2 − *x*, *z*.

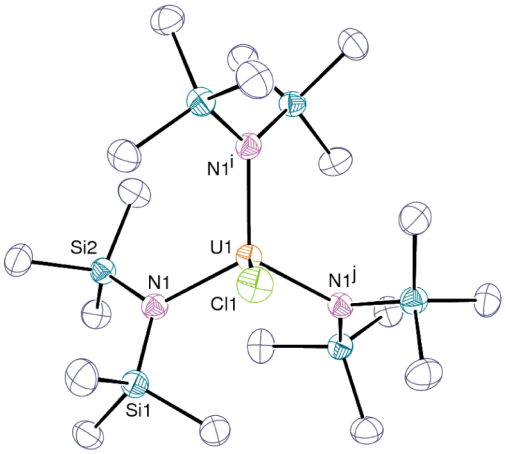

Figure 3. View of complex **3**. H atoms are omitted. Displacement ellipsoids are drawn at the 50% probability level. Symmetry codes: i, 1 − *y*, *x* − *y* + 1, *z*; j, *y* − *x*, 1 − *x*, *z*.

(0.456 Å)[17] < OTf [0.6574(12) Å], reflecting the increase of the steric interactions between X and the N* ligands with the size of X. Compounds **2** and **3**, which crystallize in the trigonal system, are isomorphous with $[UN^*_3I]$,[17] $[MN^*_3Cl]$ (M = Pb,[18] Ti, Zr, Hf[19]), and $[CeN^*_3X]$ (X = Cl, Br,[18] I[20]). The U−N(N*) distances, with a mean value of 2.23(4) Å for all of the complexes, are identical with that of 2.238(4) Å in $[UN^*_3I]$,[17] very similar to the Ce−N(N*) distances in $[CeN^*_3X]$ complexes [2.22(1) Å], and are ca. 0.13 Å smaller than the U−N(N*) distances in the U^{III} analogues, 2.362(3) Å in the carbene complex $[UN^*_3(C\{NMeCMe\}_2)]$[21] and 2.350(6) Å in

DOI: 10.1021/acs.inorgchem.5b00034
Inorg. Chem. 2015, 54, 2474−2490

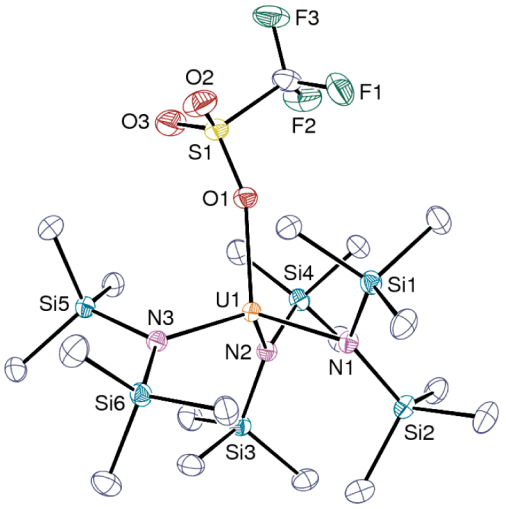

Figure 4. View of complex **4**. H atoms are omitted. Displacement ellipsoids are drawn at the 30% probability level.

$[NMe_4][UN^*_3(CN)]$,[1] in agreement with the variations of the ionic radii of the metal centers.[22] However, the striking feature of the structure of **2** is coordination of the CN group through the N atom, in contrast to the cyanide ligation mode observed in the U^{III} counterpart $[NMe_4][UN^*_3(CN)]$. The U1−N(NC) bond with a length of 2.378(9) Å is short by comparison with the U−C(CN) distances in the anionic U^{III} analogue [2.455(15) and 2.604(14) Å] and the U^{IV} complex $[NEt_4][UN^*_2(N,C)(CN)]$ [2.559(4) Å].[6] To the best of our knowledge, this U−NC linkage is unprecedented in U^{IV} compounds, but it is noteworthy that the X-ray crystal structure of the Th^{IV} complex $[Th(C_5{}^tBu_3H_2)_2(NC)(OSiMe_3)]$[23] revealed the Th−NC bonding of the CN ligand while the U−CN linkage was characterized in the U^{IV} analogue $[U(C_5{}^tBu_3H_2)_2(CN)(OSiMe_3)]$,[24] a difference that has not been commented on. In these two compounds, the Th−N [2.454(4) Å] and U−C [2.415(6) Å] distances are quite similar. The distinct ligation modes of the CN ligand in these pairs of isocyanide and cyanide complexes can be explained by the metal ion in the former being harder than that in the latter in the hard and soft acids and bases classification and having a greater affinity for the harder N end of the CN ligand. The distinct nature of the U^{IV}−NC and U^{III}−CN bonding in **2** and its U^{III} analogue has been analyzed by DFT calculations (vide infra).

Views of the metallacycles **5** and **6** are shown in Figures 5 and 6, respectively, and selected bond lengths and angles are listed in Table 2. In both centrosymmetric complexes, the metal centers are bridged by two triflate ligands, with mean U1−O distances of 2.425(9) and 2.526(2) Å in **5** and **6**, respectively. These values can be compared to those measured in the binuclear complexes $[\{U(OTf)_2(py)_2(\mu\text{-}OTf)\}_2(\mu\text{-}O)]$ [2.394(4) Å],[25] $[\{U(C_8H_8)(Cp^*)(\mu\text{-}OTf)\}_2]$ [2.50(1) Å],[26] and $[\{U(Cp^*)_2(Me)(\mu\text{-}OTf)\}_2]$[27] and $[\{U(Cp^*)(C_5Me_4H)(\mu\text{-}OTf)\}_2(\mu\text{-}O)]$ [2.51(2) Å].[28] However, the U1···$U1^i$ distance of 3.8146(3) Å in **5** is much smaller than that of 6.4491(7) Å in **6**, a shortening that is likely due to the bridging position of the CH_2 group of the *N,C* metallacycle. Such $M_2(\mu\text{-}N,C)$ linkages were previously encountered in polynuclear complexes, resulting from deprotonation of $[UN^*_2(Cl)_2]$,[29] such as $[U\{(\mu\text{-}N,C)\}_2[\mu\text{-}Li(DME)]\}_2$, where the U1···$U1^i$ distance is equal to 3.6161(12) Å, and in the binuclear compounds $[\{YN^*(THF)(\mu\text{-}N,C)\}_2]$,[30] $[\{MN^*(NMe_2)(\mu\text{-}N,C)\}_2]$ (M = Zr, Hf),[31] $[\{VN^*(\mu\text{-}N,C)\}_2]$,[32] and $[\{Cr(C_5H_5)(\mu\text{-}N,C)\}_2]$.[33] The atoms U1, C1, $U1^i$, and $C1^i$ are coplanar and form a quite perfect square [$C1{-}U1{-}C1^i = 87.15(10)°$], which is almost orthogonal, with a dihedral angle of 86.96(9)°, to the plane defined by the metal centers and the O1 and O2 atoms of the bridging triflate ligands. The U−C distances of the bridging metallacycles in **5**, which average 2.63(4) Å, are expectedly larger than that of 2.400(8) Å of the terminal U(*N,C*) moiety in **6**, which is itself at the lower limit of the range of U−C bond lengths for such metallacycles (typically equal to 2.50 Å).[5] The U−N distances, which vary from 2.190(5) to 2.256(6) Å, and the U−O(THF) distance of 2.468(5) Å are unexceptional.

Cyanido-Bridged and Bis(cyanide) Complexes $[(UN^*_3)_2(\mu\text{-}CN)]$ and $[M][UN^*_3(CN)_2]$. As in the case of the mono(cyanide) $[M][UN^*_3(CN)]$, oxidation of the U^{III} complexes $[M][(UN^*_3)_2(\mu\text{-}CN)]$ and $[M]_2[UN^*_3(CN)_2]$ [M = NR_4 or K(18-crown-6)] with a variety of oxidizing reagents (CuCl, CuI, AgI, AgOTf, $TlBPh_4$, C_5H_5NO) did not permit isolation of a pure product. Here again, the cyanido-bridged and bis(cyanide) U^{IV} complexes were readily synthesized by the addition of MCN to **1**. Thus, treatment of **1** with 0.45 mol equiv of NEt_4CN in THF afforded after the usual workup an off-white powder of **7** in 65% yield, which was recrystallized as the yellow solvate $7{\cdot}0.5Et_2O$ from Et_2O. A similar reaction with 2 mol equiv of NEt_4CN gave the bis(cyanide) $[NEt_4]$-

Table 1. Selected Bond Lengths (Å) and Angles (deg) in Complexes 1(THF) and $[UN^*_3X]$ with X = CN (2), Cl (3), and OTf (4)

	1(THF)[a]				**2**[b]		**3**[b]		**4**	
U1−O1	2.3998(18)	U2−O2	2.4310(18)	U1−N1	2.378(9)	U1−Cl1	2.593(2)	U1−O1	2.3315(18)	
U1−C1	2.892(3)	U2−C23	3.050(3)							
U1−N1	2.2371(19)	U2−N4	2.230(2)	U1−N2	2.234(4)	U1−N1	2.239(2)	U1−N1	2.232(2)	
U1−N2	2.229(2)	U2−N5	2.213(2)					U1−N2	2.218(2)	
U1−N3	2.2141(19)	U2−N6	2.2159(19)					U1−N3	2.210(2)	
N1−U1−N2	111.17(7)	N4−U2−N5	109.49(7)	N2−U1−$N2^i$	119.51(3)	N1−U1−$N1^i$	116.79(4)	N1−U1−N2	102.14(8)	
N2−U1−N3	110.14(7)	N5−U2−N6	124.60(8)					N2−U1−N3	118.28(8)	
N1−U1−N3	129.70(7)	N4−U2−N6	109.39(7)					N1−U1−N3	114.10(7)	
O1−U1−N1	98.41(7)	O2−U2−N4	126.49(7)	N1−U1−N2	94.02(10)	Cl1−U1−N1	100.44(6)	O1−U1−N1	112.43(7)	
O1−U1−N2	118.39(7)	O2−U2−N5	85.00(7)					O1−U1−N2	102.65(7)	
O1−U1−N3	86.00(7)	O2−U2−N6	101.68(7)					O1−U1−N3	106.81(7)	

[a]Values for the two independent cations. [b]Symmetry code for **2**: i, $2 - y, x - y + 1, z$. Symmetry code for **3**: i, $1 - y, x - y + 1, z$.

DOI: 10.1021/acs.inorgchem.5b00034
Inorg. Chem. 2015, 54, 2474−2490

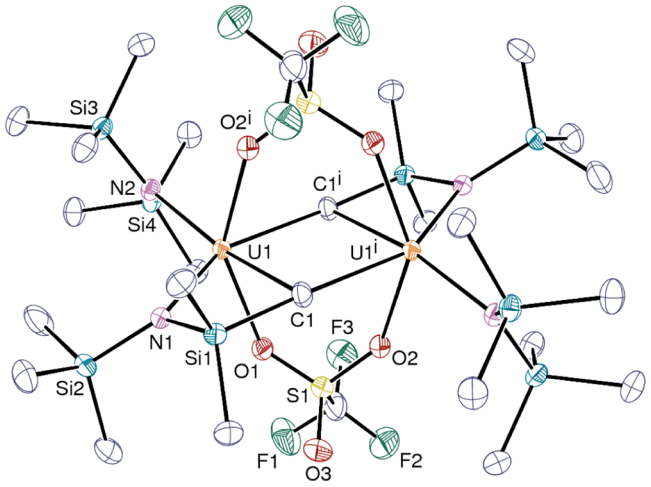

Figure 5. View of complex **5**. H atoms are omitted. Displacement ellipsoids are drawn at the 30% probability level. Symmetry code: i, 1 − *x*, −*y*, 1 − *z*.

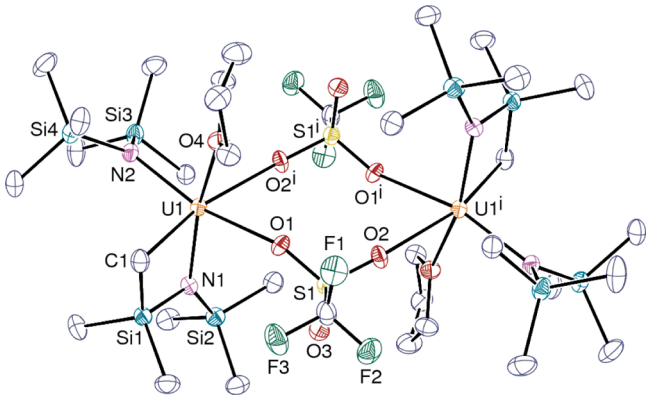

Figure 6. View of complex **6**. H atoms are omitted. Displacement ellipsoids are drawn at the 30% probability level. Symmetry code: i, −*x*, 1 − *y*, 1 − *z*.

Table 2. Selected Bond Lengths (Å) and Angles (deg) in Complexes 5 and 6

5		6	
U1−C1	2.661(3)	U1−C1	2.400(8)
U1−C1^{i}	2.604(3)	U1−O4	2.468(5)
U1−N1	2.190(3)	U1−N1	2.200(6)
U1−N2	2.254(2)	U1−N2	2.256(6)
U1−O1	2.418(3)	U1−O1	2.528(5)
U1−O2^{i}	2.432(3)	U1−O2^{i}	2.525(5)
C1−U1−N1	70.59(9)	C1−U1−N1	73.2(3)
C1^{i}−U1−N1	154.37(10)	C1−U1−N2	92.5(3)
C1−U1−N2	161.53(12)	C1−U1−O2^{i}	159.0(2)
C1−U1−C1^{i}	87.15(10)	N1−U1−N2	110.9(2)
N1−U1−N2	106.97(9)	N1−U1−O4	155.1(2)
O1−U1−O2^{i}	146.66(7)	N2−U1−O1	159.9(2)
U1−C1−U1^{i}	92.86(10)	O1−U1−O2^{i}	72.71(18)

Symmetry code for **5**: i, 1 − *x*, −*y*, 1 − *z*. Symmetry code for **6**: i, −*x*, 1 − *y*, 1 − *z*.

$[UN^*_3(CN)_2]$ (**8**), which was isolated as a pink powder in 58% yield. The reaction of **1** with an excess of KCN led to the formation of a greenish powder of $K[UN^*_3(CN)_2]$ in 63% yield, and green crystals of $[K(THF)_4][UN^*_3(CN)_2]$ (**9**) were formed by crystallization from THF. Not surprisingly, the $[UN^*_3(CN)_2]^-$ anion was also obtained by the addition of CN^- to the mono(cyanide) **2**. Rapid exchange of the CN ligand between the mono- and bis(cyanide) complexes was revealed by the ^{1}H NMR spectra to be mixtures of these complexes in THF-d_8, which exhibited average resonances at δ between −3.07 and −1.40, values that correspond to the N* ligands of **2** and **8**, respectively.

Attempts at the synthesis of uranium(V) cyanide complexes by the oxidation of **2**, **8**, or **9** were unsuccessful. In one reaction of **9** with $CuBr_2$, red crystals of $[UN^*_3(Br)_2]$ were isolated and characterized by ^{1}H NMR spectroscopy and X-ray diffraction analysis.[34] It is also noteworthy that $[UN^*_3(CN)_2]$ could not be synthesized by the substitution of $[UN^*_3X_2]$ (X = F, Cl, Br) with cyanide ligands, a difficulty that was explained by unfavorable thermodynamic factors.[35] Only three uranium(V) cyanide complexes were reported: $[N^nBu_4]_2[U(Cp^*)_2(CN)_5]$,[36] $[Na(15\text{-crown-}5)][UN^*(N,O)_2(CN)]$ [*N*,*O* = $OC(=CH_2)SiMe_2N(SiMe_3)$][6] and $[NEt_4][UON^*_3(CN)]$.[35]

Views of the cation of the cyanide-bridged complex **7** and the anion of the bis(cyanide) **9** are shown in Figures 7 and 8, respectively, and selected bond distances and angles are listed in Table 3; the structural parameters of **10**, which was obtained from the oxidation of $[K(18\text{-crown-}6)][UN^*_3(CN)]$ with pyridine *N*-oxide (vide supra), are also given in Table 3, and a view of this compound is presented in Figure 9. The structures of **7** and **9** resemble those of the anionic fragments in the corresponding U^{III} complexes $[K(18\text{-crown-}6)][(UN^*_3)_2(\mu\text{-CN})]$ and $[K(18\text{-crown-}6)]_2[UN^*_3(CN)_2]$.[1] The U1 and U2 atoms in **7** are in a pseudotetrahedral configuration, at a distance of 0.550(4) and 0.698(3) Å from the plane of the nitrogen amide ligands, while the U1 atom in **9** lies in this plane, being in a quite perfect trigonal-bipyramidal environment. The U−N(N*) distances, which average 2.204(9) and 2.252(3) Å in **7** and **9**, respectively, are smaller than those of 2.367(10) and 2.386(10) Å in the U^{III} counterparts, in line with variation of the radii of the U^{IV} and U^{III} ions. The mean U−C/N(CN) distance of 2.562(13) Å in **7** is larger than that in the U−N(CN) distance of 2.493(4) and 2.468(3) Å in **9** and **10**, respectively. In the latter two complexes, the K−C distances average 2.930(5) Å in **9** and 2.916(13) Å in **10**. However, the most striking feature in the structures of the uranium(III) and

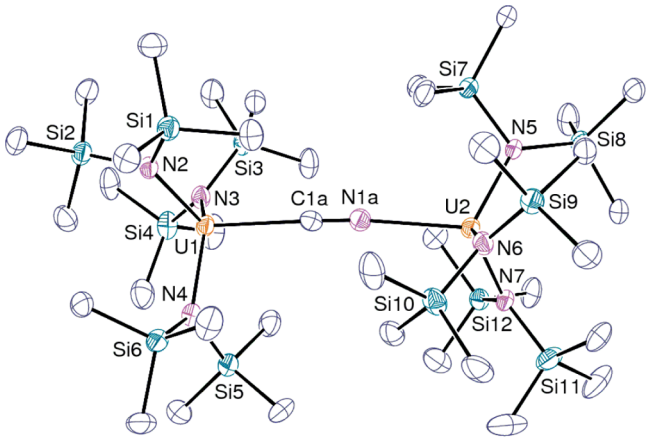

Figure 7. View of the cation in 7·0.5Et_2O. H atoms are omitted. Displacement ellipsoids are drawn at the 30% probability level. One particular position of the disordered cyanide is represented.

DOI: 10.1021/acs.inorgchem.5b00034
Inorg. Chem. 2015, 54, 2474−2490

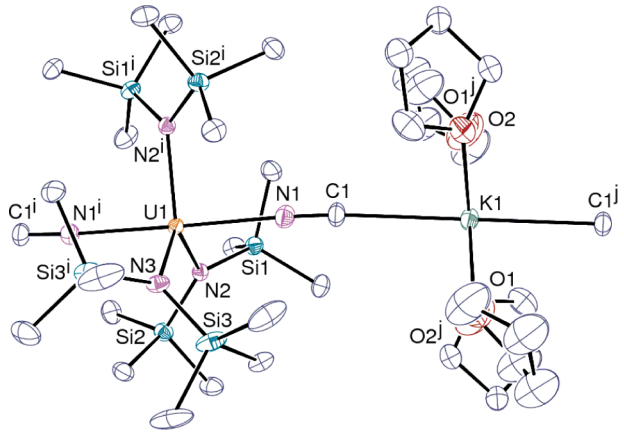

Figure 8. View of complex **9**. H atoms are omitted. Displacement ellipsoids are drawn at the 20% probability level. Symmetry codes: i, $1 - x, y, {}^{3}/_{2} - z$; j, ${}^{3}/_{2} - x, {}^{3}/_{2} - y, 2 - z$.

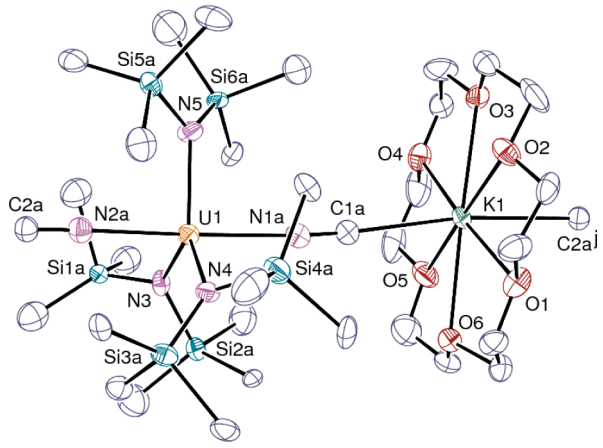

Figure 9. View of complex **10**. H atoms are omitted. Displacement ellipsoids are drawn at the 20% probability level. Only one position of the disordered parts is represented. Symmetry codes: i, $x, y, z + 1$; j, $x, y, z - 1$.

uranium(IV) bis(cyanide) compounds is, as in the case of the mono(cyanide) complexes, the distinct ligation mode of the CN ligand, U^{III}–CN versus U^{IV}–NC (Scheme 3). The U–N(NC) distance of 2.493(4) Å in **9** is 0.11 Å larger than in the mono(cyanide) **2**, reflecting variation in the coordination number and charge of the complexes. The CN^- ligand in **10** has been refined as a mixture of cyanide and isocyanide, but the structure determination is of lower quality because of substantial disorder (see the Experimental Section), so that the modeling of this anion must be taken with caution. In addition, the ∼0.8 Å difference between the U^{III}–C and U^{IV}–N(CN) distances in the mono(cyanide) $[UN^*_3(CN)]^q$ complexes (q = 1−, 0)[1] is in the range of expected values by changing the oxidation state of the metal center by one unit in an ionic model.

The IR spectra of the mono- and bis(cyanide) complexes **2** and **8** show strong absorption bands assigned to the ν(CN) stretching frequencies at 2044 and 2058 cm^{-1}, respectively, while the IR vibrational frequency of the cyanide ion in NEt_4CN is 2050 cm^{-1}. These values can be compared with those of the mononuclear U^{IV} compounds $[NEt_4][U(Cp^*)_2(CN)_3]$ (2053 and 2188 cm^{-1}),[7] $[NR_4]_3[U(Cp^*)_2(CN)_5]$ (2091 cm^{-1}),[36] $[U(C_5{}^tBu_3H_2)_2(CN)(OSiMe_3)]$ (2040 cm^{-1}),[24] and $[NEt_4][U(C_8H_8)_2(CN)]$ (2073 cm^{-1}),[37] and they suggest the absence of π back-bonding from the U^{4+} ion to the cyanide ligand.

Scheme 3. U–NC versus U–CN Coordination Mode in the Complexes $[U^{III}N^*_3(CN)_2]^{2-}$, $[U^{IV}N^*_3(NC)_2]^-$, $[U^{IV}N^*(N,N)(CN)_2]^-$, and $U^{IV}N^*_3(NC)$

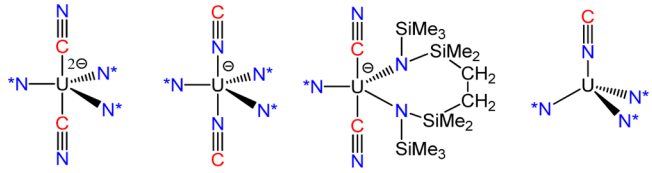

Table 3. Selected Bond Lengths (Å) and Angles (deg) in Complexes 7·0.5Et_2O, 9, and 10

7·0.5Et_2O				9[a]		10[a]	
U1–C1a	2.549(8)	U2–N1a	2.574(7)	U1–N1	2.493(4)	U1–N1a	2.466(9)
				K–C1	2.930(5)	K–C1a	2.929(11)
						U1–N2a	2.471(9)
						K^i–C2a	2.904(11)
U1–N2	2.210(6)	U2–N5	2.197(5)	U1–N2	2.254(3)	U1–N3	2.316(16)
U1–N3	2.219(6)	U2–N6	2.205(6)	U1–N3	2.248(5)	U1–N4	2.201(14)
U1–N4	2.193(6)	U2–N7	2.206(6)			U1–N5	2.246(7)
N2–U1–N3	107.9(2)	N5–U2–N6	113.5(2)	N2–U1–N3	118.55(9)	N3–U1–N4	118.2(3)
N3–U1–N4	126.7(2)	N6–U2–N7	110.7(2)	N2–U1–$N2^i$	122.89(18)	N4–U1–N5	122.9(7)
N2–U1–N4	107.0(2)	N5–U2–N7	107.1(2)			N3–U1–N5	118.8(7)
C1a–U1–N2	112.5(2)	N1a–U2–N5	110.4(2)	N1–U1–N2	89.91(13)	N1a–U1–N3	95.7(4)
C1a–U1–N3	106.7(2)	N1a–U2–N6	105.0(2)	N1–U1–$N2^i$	89.15(13)	N1a–U1–N4	88.5(5)
C1a–U1–N4	95.5(2)	N1a–U2–N7	110.2(2)	N1–U1–N3	90.99(10)	N1a–U1–N5	89.8(3)
				N1–U1–$N1^i$	178.0(2)	N2a–U1–N3	93.5(5)
						N2a–U1–N4	84.5(6)
						N2a–U1–N5	88.4(3)
						N1a–U1–N2a	170.3(5)

[a]Symmetry code for **9**: i, $1 - x, y, {}^{3}/_{2} - z$. Symmetry code for **10**: i, $x, y, z - 1$.

DOI: 10.1021/acs.inorgchem.5b00034
Inorg. Chem. 2015, 54, 2474–2490

The ν(CN) frequencies of the cyano-bridged complexes **7** and **9** at 2115 and 2078 cm^{-1}, respectively, are expectedly larger than those corresponding to the terminal cyanide ligands in **2** and **8**. Indeed, the ν(CN) frequencies of cyanide bridges M−CN−M′ are generally shifted to higher energies than those of terminal cyanides M−CN.[38] The larger ν(CN) values for **9** likely reflect the presence of the U−CN−K linkages, with these being absent in **8**, which involves the noncoordinating NEt_4 cation.[38] The values for the U^{IV} complexes **7** and **9** are also larger than those measured for the U^{III} counterparts $[NEt_4][(UN^*_3)_2(\mu\text{-CN})]$ (2096 cm^{-1}) and $[K(18\text{-crown-}6)]_2[UN^*_3(CN)_2]$ (2063 cm^{-1}).[1] This is most probably to be accounted for by the increase of the ν(CN) frequency generally observed with the increasing oxidation state of the metal ion rather than by the slightly more covalent character of the U^{III}−CN bonding, which is devoid of any U^{III}-to-cyanide π^* back-donation according to DFT studies on trivalent $[U^{III}N^*_3X_2]^{2-}$ compounds.[1] In contrast, the ν(CN) stretching frequencies of **2** and **8** at 2044 and 2058 cm^{-1} are smaller than or equal to those of the U^{III} analogues $[NEt_4][UN^*_3(CN)]$ (2057 cm^{-1}) and $[N^nBu_4]_2[UN^*_3(CN)_2]$ (2058 cm^{-1}).[1] This feature, difficult to explain, could reflect the distinct U−CN and U−NC ligation modes in the corresponding U^{III} and U^{IV} complexes, although these U−ligand bonds are predominantly ionic (vide infra).

It is important to note that the U^{III}−CN versus U^{IV}−NC coordination mode observed in the tris(silylamide) UN^*_3 complexes, as well as the Ce^{III}/U^{III} differentiation previously studied,[1] cannot be considered as a general feature. Indeed, it seems strongly related to the electronic structure of the complexes and the coordination geometry of the ligands. For example, the M−C bonding mode was unambiguously determined in the series of bis(Cp*) complexes $[N^nBu_4][U^{IV}(Cp^*)_2(CN)_3]$ and $[N^nBu_4]_2[M^{III}(Cp^*)_2(CN)_3]$ (M = U, Ce),[7,36,39] which are much more electron-rich than the tris(N*) compounds. In the U^{VI} compound $[UO_2(CN)_5]^{3-}$, the lower charge of the uranyl ion and the trianionic charge of the whole complex render the metal softer, thus favoring U−C coordination of the cyanide ion.[40] Moreover, whereas the *N*,*N* metallacyclic bis(cyanide) complex $[NEt_4][UN^*(N,N)(CN)_2]$ (**11**) [*N*,*N* = $(Me_3Si)NSiMe_2CH_2CH_2SiMe_2N(SiMe_3)$][6] is a close analogue of **10** with similar structure (Scheme 3), the CN ligands are also unambiguously coordinated through the C atoms. This striking and unexpected difference, which is apparently related to slight variations in the geometrical parameters, in particular the N−U−N angles of the amido ligand set, which deviate from 120° by 4−10°, was explained by DFT analysis.

DFT Molecular Geometry Optimization of the Complexes. To investigate further the cyanide coordination preference to the U^{III} or U^{IV} metal center, the two mono- and bis(cyanide/isocyanide) complexes $[UN^*_3X]^q$ (q = 1−, 0) and $[UN^*_3X_2]^q$ (q = 2−, 1−) ($U^{3+/4+}$; X = CN, NC) were first considered. Recently, comparative studies on actinide compounds using various DFT-based techniques[41a] demonstrated that generalized gradient approximation functionals (e.g., BP86 or PBE; see the Computational Details) give results with comparable reliability to that of hybrid ones (e.g., B3LYP) regarding molecular geometries.[41b] For our part, we carried out computations in the framework of the relativistic zeroth-order regular approximation (ZORA) using the BP86 functional and the polarized triple-ζ Slater basis set (TZP). As previously stated,[1,42] ZORA/BP86/TZP-computed geometries are in good agreement with X-ray structures. Thus, all structures considered here have been computed at this level of theory. The computed U^{III}−CN, U^{IV}−NC, U−N*, and C−N bond lengths for the actual mono- and bis(cyanide/isocyanide) complexes, respectively, are reported in Tables 4 and 5. Their hypothetical U^{III}−NC and U^{IV}−CN analogues were also computed and considered for comparison.

The optimized structures of the $[UN^*_3X]^q$ (q = 1−, 0) and $[UN^*_3X_2]^q$ (q = 2−, 1−) complexes are depicted in Figures 10 and 11, respectively, and can be compared with the available X-ray crystallographic data of the actual U^{III}−CN and U^{IV}−NC complexes **2** and **9**. First, the computed geometries of the actual U^{III}−CN and U^{IV}−NC systems are in good agreement with available X-ray data with a slight discrepancy, reaching ca. 0.06 Å, for the metal−ligand bond distance in the case of the $U^{IV}(NC)_2$ complex (Table 5). This good agreement shows once again the reliability of the ZORA/BP86/TZP method in computing molecular f complex geometries.[1,42] The shortening of the metal−ligand bond distances when passing from U^{III} to U^{IV}, in line with uranium ionic radii variation,[22] is well predicted by computation. Moreover, the C−N bond length undergoes no significant change in the U^{III} and U^{IV} complexes, suggesting mainly cyanide-to-metal σ donation, with no π-back-donation effects, in agreement with the experimental findings. In addition, the computed U−C−N and U−N−C bond angles are indicative of linear coordination with an unperturbed multiple C−N bond. It is also noteworthy that the computed N*−U−X (X = CN, NC) bond angles are significantly smaller in the U^{IV} complexes than in the U^{III} analogues (92.8 vs 100.8°). This trend is also observed experimentally for the actual systems, where the N*−U^{III}−CN and N*−U^{IV}−NC bond angles are equal to 101.1 and 94.0°, respectively, differences that could result from a slightly stronger donation ability of CN over NC ligands toward U^{III}, while the trend is converse toward U^{IV} metal centers. Electronic structure analysis will shed light on these points.

The optimized structure of the metallacyclic uranium(IV) bis(cyanide) complex $[UN^*(N,N)(CN)_2]^-$ is shown in Figure 12. As aforementioned, the striking difference with the $[U^{IV}N^*_3X_2]^-$ complex is the U^{IV}−CN coordination. The computed bond lengths (Table 5) compare very well with the X-ray data.[6] The computed N*−U−N* angles, equal to 114.2−130.1°, deviate significantly from 120°, in agreement with the experimental data.[6] This structural feature is also predicted for the isocyanide hypothetical analogue $[UN^*(N,N)(NC)_2]^-$. The striking difference in coordination between the $[UN^*(N,N)(CN)_2]^-$ complex and the other U^{IV} species could not be directly related to these angle variations.

Electronic Structures of the Complexes. As previously stated,[43] the cyanide or isocyanide CN^-/NC^- anions are strong

Table 4. ZORA/BP86/TZP Relevant Optimized Averaged Metal−Ligand Bond Distances (Å) and Angles (deg) of the Mono(cyanide/isocyanide) Complexes $[UN^*_3X]^q$ (q = 1−, 0) ($U^{3+/4+}$; X = CN/NC) with Available X-ray Data

CN/NC structure	⟨U−X⟩	⟨C−N⟩	⟨U−N*⟩	N*−U−C/N
$U^{III}N^*_3$−CN	2.500	1.177	2.349	100.8
X-ray[1] for the U^{III} complex	**2.455(15)**	**1.17(2)**	**2.348(5)**	**101(1)**
$U^{IV}N^*_3$−CN	2.462	1.172	2.252	91.3
$U^{III}N^*_3$−NC	2.384	1.187	2.350	100.7
$U^{IV}N^*_3$−NC	2.324	1.186	2.256	92.8
X-ray for 2	**2.378(9)**	**1.118(15)**	**2.234(4)**	**94.02(10)**

DOI: 10.1021/acs.inorgchem.5b00034
Inorg. Chem. 2015, 54, 2474−2490

Table 5. ZORA/BP86/TZP Relevant Optimized Averaged Metal−Ligand Bond Distances (Å) and Angles (deg) of the Bis(cyanide/isocyanide) Complexes $[UN^*_3X_2]^q$ (q = 2−, 1−) and $[UN^*(N,N)X_2]^-$(X = CN, NC) with Available X-ray Data

CN/NC structure	⟨U−X⟩	⟨C−N⟩	⟨U−N*⟩	⟨N*−U−N*⟩
$U^{III}N^*_3-(CN)_2$[1]	2.604	1.180	2.378	120.0
X-ray[1] for the U^{III} complex	**2.62(6)**	**1.168(3)**	**2.39(1)**	**119.9(4)**
$U^{IV}N^*_3-(CN)_2$	2.576	1.173	2.280	120.1
$U^{III}N^*_3-(NC)_2$[1]	2.483	1.185	2.389	119.9
$U^{IV}N^*_3-(NC)_2$	2.429	1.183	2.293	120.1
X-ray for 9	**2.493(4)**	**1.154(7)**	**2.252(3)**	**120.5(5)**
$U^{IV}N^*(N,N)-(CN)_2$	2.575	1.174	2.241	114.2−130.1
X-ray[6] for 11	**2.50(2)**	**1.14(1)**	**2.266(1)**	**114.7(2)−130.3(2)**
$U^{IV}N^*(N,N)-(NC)_2$	2.441	1.183	2.250	114.3−130.0

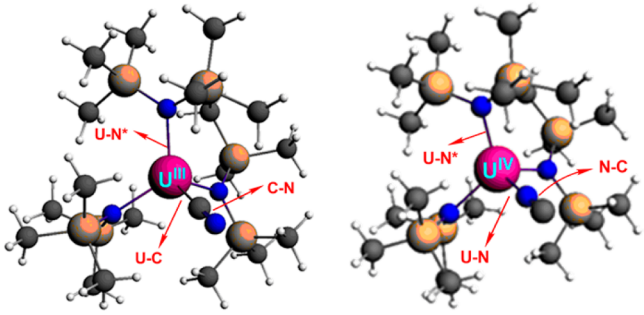

Figure 10. ZORA/BP86/TZP-optimized structures of the mono(cyanide/isocyanide) complexes $[UN^*_3X]^q$ (q = 1−, 0; X = CN, NC).

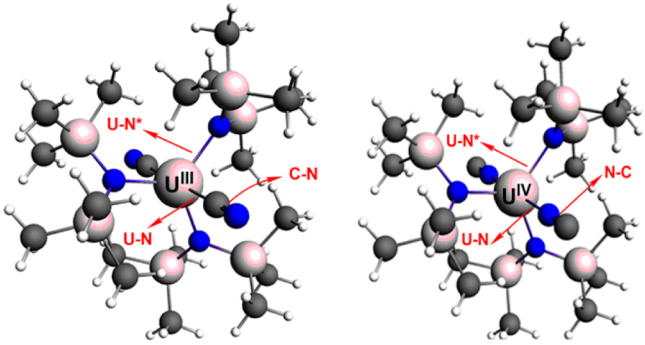

Figure 11. ZORA/BP86/TZP-optimized structures of the bis(cyanide/isocyanide) complexes $[UN^*_3X_2]^q$ (q = 2−, 1−; X = CN, NC).

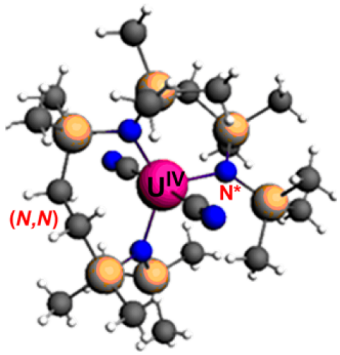

Figure 12. ZORA/BP86/TZP-optimized structure of the metallacyclic uranium(IV) bis(cyanide) complex $[UN^*(N,N)(CN)_2]^-$.

σ donors. This originates from σ donation of either the C-localized upper orbital of CN^- or the lower N-localized orbital of NC^- with N major character. Their coordination preference toward U^{VI} (d^0f^0) in uranyl systems UO_2^{2+} was investigated by Bursten et al.,[43a] who concluded that metal-based orbitals match energetically better with the C-localized σ orbital of the cyanide ligand, making it a much more effective donor than the N-localized σ orbital. Our previous work on cyanide/isocyanide coordination related to Ln^{III}/An^{III} differentiation revealed distinct coordination modes of the CN group.[1] It appeared that the better energy matching between 6d/5f U and ligand orbitals plays a significant role in the metal−ligand coordination preference of the cyanide/isocyanide ligands toward the U^{III}/Ce^{III} pair in the $[MN^*_3X_2]^{2-}$ complexes (M = Ce, U; X = CN, NC), and the U−CN versus Ce−NC coordination was well corroborated by consideration of the binding energies of these ligands to the metal ions and by natural population analysis (NPA), the quantum theory of atoms in molecules (QTAIM), and bond order analyses. Thus, the distinct coordination of the CN versus NC ligands toward the U^{III}/U^{IV} pair can also be related to the energy matching and stronger σ-donating ability of the cyanide and isocyanide ligands.

The computed Mayer[44] and Nalewajski−Mrozek (NM)[45] bond indices (see the Computational Details) for the U−C/N and C−N bonds are reported in Table 6. As expected, the NM approach, which accounts for ionic and covalent contributions, gives greater metal−ligand bond orders (up to 2 times) than the Mayer approach. For the C−N/N−C bonds, the ionic character is low, so that the NM and Mayer indices get closer. It is worth noting that, for all systems, Mayer analysis consistently gives larger U−X bond orders (X = CN, NC) for the U^{IV} complexes than for their U^{III} congeners, in agreement with the computed U^{III} to U^{IV} bond shortening. Interestingly, in the case of the mono(cyanide/isocyanide) $[UN^*_3X]^q$ (q = 1−, 0) systems, systematically larger Mayer bond orders for cyanide $U^{III/IV}$−CN coordination than for isocyanide $U^{III/IV}$−NC coordination are observed. On the contrary, NM bond orders are in line with the different coordination preferences of the U^{III} and U^{IV} ions. Indeed, a significantly higher bond order is obtained for U^{III}−CN, 1.176 versus 0.994 for U^{III}−NC, likely indicating a significantly stronger coordination preference of cyanide than isocyanide toward U^{III}. Such a good correlation between NM bond orders and the coordination preference has already been observed considering the Ce^{III}/U^{III} pair,[1] thus confirming the reliability of the NM approach.[46]

Moreover, the reverse is obtained for U^{IV} systems because the cyanide U^{IV}−CN NM bond order is significantly smaller than the isocyanide U^{IV}−NC bond order (1.082 vs 1.245), correlating well with the observed coordination. Furthermore, in the bis(cyanide/isocyanide) $[UN^*_3X_2]^q$ (q = 2−, 1−) complexes, the computed NM bond orders are larger for the $U^{III}(CN)_2$ coordination than for the $U^{III}(NC)_2$ one (0.814 vs

DOI: 10.1021/acs.inorgchem.5b00034
Inorg. Chem. 2015, 54, 2474−2490

Table 6. ZORA/BP86/TZP NM and Mayer Average Bond Orders for the Mono- and Bis(cyanide/isocyanide) Complexes $[UN^*_3X]^q$ (q = 1−, 0), $[UN^*_3X_2]^q$ (q = 2−, 1−), and $[UN^*(N,N)X_2]^-$ (X = CN, NC)[a]

			atom−atom bond orders			
			Mayer		NM	
CN/NC structure		⟨d⟩ (Å)	⟨U−X⟩	⟨C−N/N−C⟩	⟨U−X⟩	⟨C−N/N−C⟩
$U^{III}N^*_3$−CN	Q	2.500	0.591	2.801	1.176	2.935
$U^{IV}N^*_3$−CN	T	2.462	0.612	2.833	1.082	3.019
$U^{III}N^*_3$−NC	Q	2.384	0.486	2.463	0.994	2.981
$U^{IV}N^*_3$−NC	T	2.324	0.605	2.357	1.245	2.857
$U^{III}N^*_3$−$(CN)_2^1$	Q	2.604	0.614	2.814	0.814	3.095
$U^{IV}N^*_3$−$(CN)_2$	T	2.576	0.628	2.864	0.896	3.016
$U^{III}N^*_3$−$(NC)_2^1$	Q	2.483	0.439	2.602	0.778	3.034
$U^{IV}N^*_3$−$(NC)_2$	T	2.429	0.467	2.487	1.037	2.891
$U^{IV}N^*(N,N)$−$(CN)_2$	T	2.575	0.610	2.873	0.939	2.899
$U^{IV}N^*(N,N)$−$(NC)_2$	T	2.441	0.496	2.552	0.820	3.006

[a]Q = quartet. T = triplet.

0.778)[1] and smaller for $U^{IV}(CN)_2$ than for $U^{IV}(NC)_2$ (0.896 vs 1.037). These results show that, for the systems under study, the observed U^{III}−CN versus U^{IV}−NC coordination preferences can be deduced from the highest NM bond orders.

To get a clearer picture of covalency in U−CN/NC coordination, electronic structure analyses including NPA[47a] and QTAIM[47b] descriptors have been considered. NPA and QTAIM approaches have proved to be more reliable than the Mulliken population analysis.[47c] QTAIM bond critical point (BCP) properties (electron and energy densities ρ_c and H_c) have also been calculated using the *ADF* program.[47k,l] In particular, for f-element complexes, these two topological approaches were used to probe the covalency and gave results in good agreement with the experimental trends.[47d−f] The results of NPA and QTAIM calculations, computed at the ZORA/BP86/TZP level for both the U−CN and U−NC coordination modes in the mono- and bis(cyanide/isocyanide) $[UN^*_3X]^q$ (q = 1−, 0) and $[UN^*_3X_2]^q$ (q = 2−, 1−) complexes, are reported in Table 7. The natural metal charge as well as the metallic spin population ρ_U are presented. The latter property is computed as the difference between the total α- and β-spin electronic populations of the metal. The QTAIM descriptors, i.e., electron (ρ_c) and energy density (H_c) data, at the metal−ligand BCPs for $U^{III/IV}$−CN/NC bonds are also given. As expected, inspection of the NPA results for the $[UN^*_3X]^q$ (q = 1−, 0; X = CN/NC) complexes shows significantly smaller natural metal charges than the formal value 3 of the U^{III} ion, independent of the U−CN or U−NC coordination (for instance, 2.13/2.15 for U^{III} instead of 3), indicating a strong σ donation of the ligand. Interestingly, the metal spin population of the U^{III} complex, which is a $5f^3$ species, is lower than 3, whereas this population is higher than 2 in the case of the U^{IV} $5f^2$ complex. This means that for the latter complexes a small negative spin density is spread over the ligands as noted previoulsy.[40] Moreover, the comparison between mono- and bis(cyanide/isocyanide) systems shows that metallic net charges become smaller for the latter complexes (2.13 vs 2.07 for U^{III}−CN and 2.46 vs 2.40 for U^{IV}−NC). It appears also that, for the U^{III}/U^{IV} $[UN^*_3X]^q$ (q = 1−, 0) pairs, the NPA charges show only a slight difference between the cyanide and isocyanide coordination (e.g., 2.13 vs 2.15 for U^{III}−CN/NC). Nevertheless, as suggested by bond order analysis (Table 6), the U^{III}−CN coordination is significantly stronger than the U^{III}−NC one, and the opposite is obtained for the U^{IV} complexes, in agreement with the observed coordination preference. Furthermore, the stronger donation ability and covalent bonding of the cyanide over isocyanide toward U^{III} is also highlighted by the QTAIM approach. Indeed, as given by the BCPs, the computed electron density (ρ_c) is slightly higher for the U^{III}−CN coordination than for the U^{III}−NC one (0.075 vs 0.070), and the energy density (H_c) data are meaningfully more negative (−0.052 vs −0.034). Thus, the covalent contribution appears to be more important for the cyanide U^{III}−CN coordination than for the isocyanide U^{III}−NC coordination. Moreover, in the U^{IV} case, as corroborated by bond orders, the U^{IV}−NC electron density ρ_c is higher than that in U^{IV}−CN (e.g., 0.042 vs 0.037), indicating a slightly more covalent character in the former. More interestingly, the critical electron density (ρ_c) is slightly larger for the actual uranium(IV) bis(isocyanide) complex $[UN^*_3(NC)_2]^-$ than for its hypothetical bis(cyanide) congener $[UN^*_3(CN)_2]^-$ (0.067 vs 0.059). These results correlate well with the stronger isocyanide NC σ-donation ability toward U^{IV} and its experimentally observed coordination preference.

A comparison of all of the uranium(III) and uranium(IV) mono(cyanide/isocyanide) pairs shows a decrease in the electron density ρ_c (e.g., 0.075 vs 0.037 from U^{III}−CN to U^{IV}−CN), suggesting also a decrease in the covalency. The same trend is noted with the isocyanide $U^{III/IV}$−NC complexes

Table 7. ZORA/BP86/TZP NPA and QTAIM Results for the Mono- and Bis(cyanide/isocyanide) Complexes $[UN^*_3X]^q$ (q = 1−, 0), $[UN^*_3X_2]^q$ (q = 2−, 1−), and $[UN^*(N,N)X_2]^-$ (X = CN, NC)

			QTAIM U−C/N	
U−(CN/NC) structure	natural spin population ρ_U	NPA net charge q_U	ρ_c (e/bohr^3)	H_c (au)
$U^{III}N^*_3$−CN	2.91	2.13	0.075	−0.052
$U^{IV}N^*_3$−CN	2.12	2.41	0.037	−0.013
$U^{III}N^*_3$−NC	2.92	2.15	0.070	−0.034
$U^{IV}N^*_3$−NC	2.12	2.46	0.042	−0.026
$U^{III}N^*_3$−$(CN)_2^1$	2.88	2.07	0.027	−0.026
$U^{IV}N^*_3$−$(CN)_2$	2.10	2.34	0.059	−0.023
$U^{III}N^*_3$−$(NC)_2^1$	2.85	2.18	0.025	−0.018
$U^{IV}N^*_3$−$(NC)_2$	2.09	2.40	0.067	−0.043
$U^{IV}N^*(N,N)$−$(CN)_2$	2.03	2.28	0.032	−0.021
$U^{IV}N^*(N,N)$−$(NC)_2$	2.01	2.36	0.029	−0.013

DOI: 10.1021/acs.inorgchem.5b00034
Inorg. Chem. 2015, 54, 2474−2490

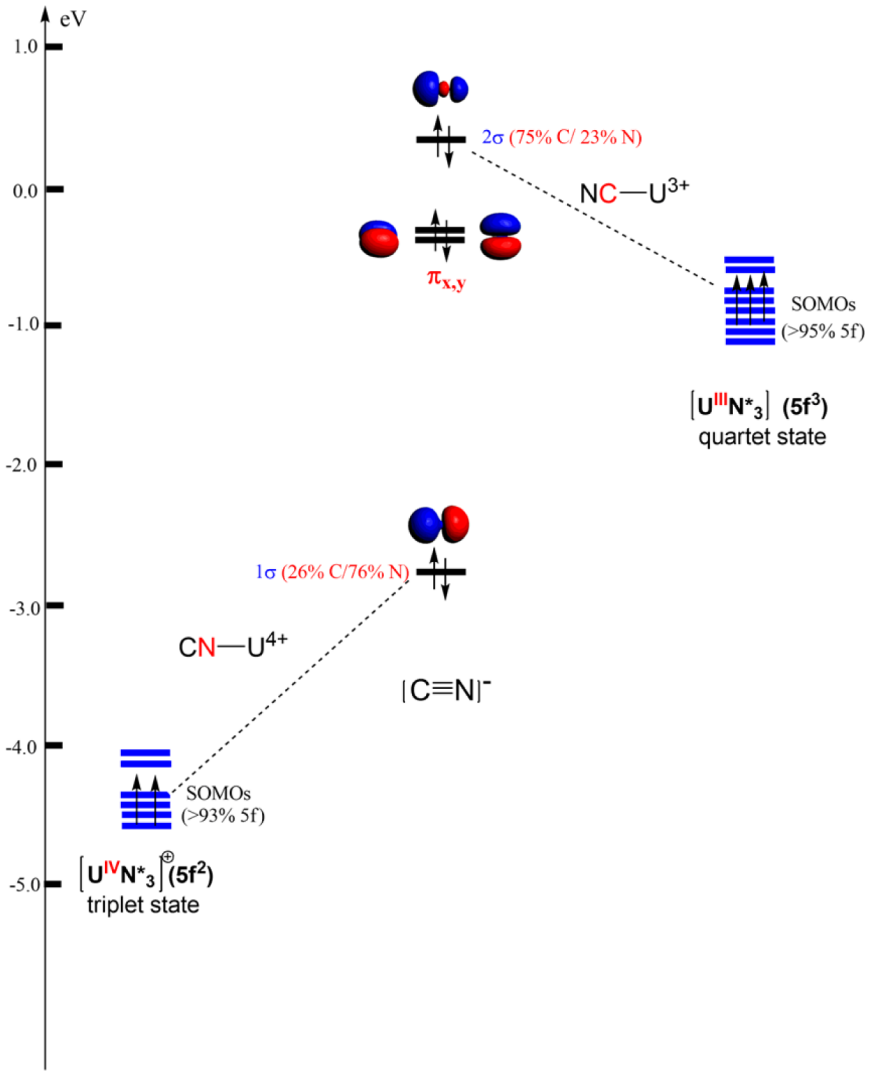

Figure 13. ZORA/BP86/TZP interaction diagram for the $[UN^*_3]^q$ (q = 1, 0) molecular fragments and the cyanide CN^- ligand. In this diagram, the U^{III} $[UN^*_3]$ and U^{IV} $[UN^*_3]^+$ levels are displayed on the right and left, respectively, and the cyanide ion MOs are given in the middle.

(i.e., 0.070 vs 0.042 for ρ_c). As suggested by Kaltsoyannis et al.,[47d,h] this phenomenon can be related to the better energy matching between the metallic 6d/5f and ligand orbitals. In fact, the decrease of the covalency (weaker orbital mixing) when passing from U^{III}−CN to U^{IV}−CN is attributed to the smaller σ-donation ability of the C-localized upper orbital toward a deeper U^{IV} 6d/5f shell. The stronger σ-donation ability of isocyanide in the case of U^{IV}−NC than that of cyanide in U^{IV}−CN is also explained by the better energy matching between U^{IV} 6d/5f and N-localized orbitals. This stronger interaction leads to a slight increase in the covalency factor, i.e., the electron density ρ_c (0.037 for U^{IV}−CN vs 0.042 for U^{IV}−NC). This explains the observed coordination preference of CN/NC toward the U^{III}/U^{IV} pair in the actual $[UN^*_3X]^q$ (q = 1−, 0) systems. However, in the bis(cyanide/isocyanide) $[UN^*_3X_2]^{2-}$ compounds, the opposite trend is observed when passing from U^{III} to U^{IV}. Indeed, a comparison between the $U^{III}(CN)_2$ and $U^{IV}(CN)_2$ complexes shows a significant increase in the electron density ρ_c (0.027 vs 0.059), suggesting a more covalent contribution in the latter. The same trend is noted with the bis(isocyanide) $U^{III/IV}(NC)_2$ derivatives (0.025 vs 0.067).

Overall, it appears that the stronger σ-donation ability (due to better energy matching) correlates with the increase in the covalent contribution (orbital mixing), which accounts for a significant part of the $U^{III/IV}$−CN/NC bonding. It is also worth noting that QTAIM data clearly highlight the slight role of covalency in the observed cyanide CN versus isocyanide NC coordination preference toward the U^{III}/U^{IV} pair. In fact, as noted in previous works on f complexes,[47g,h] the BCP values provided from the QTAIM method are small and suggest weak covalency, thus indicating dominant ionic metal−ligand bonding.

Turning back to the $[UN^*(N,N)X_2]^-$ complex, the major variations of the Mayer and NM U−C/N bond indices between the cyanide and isocyanide derivatives $[UN^*(N,N)X_2]^-$ are similar to those obtained for the corresponding $[UN^*_3X_2]^-$ (X = CN, NC) complexes (Table 6). Here again, the observed cyanide coordination for the metallacyclic complex is well predicted with a metal−ligand NM bond order larger for U−CN than for U−NC (0.939 vs 0.820). Indeed, to further assess this point, the QTAIM data (Table 7) considering the distinct coordination modes of the cyanide ligand in the two actual compounds indicate that the electron and energy densities ρ_c

DOI: 10.1021/acs.inorgchem.5b00034
Inorg. Chem. 2015, 54, 2474−2490

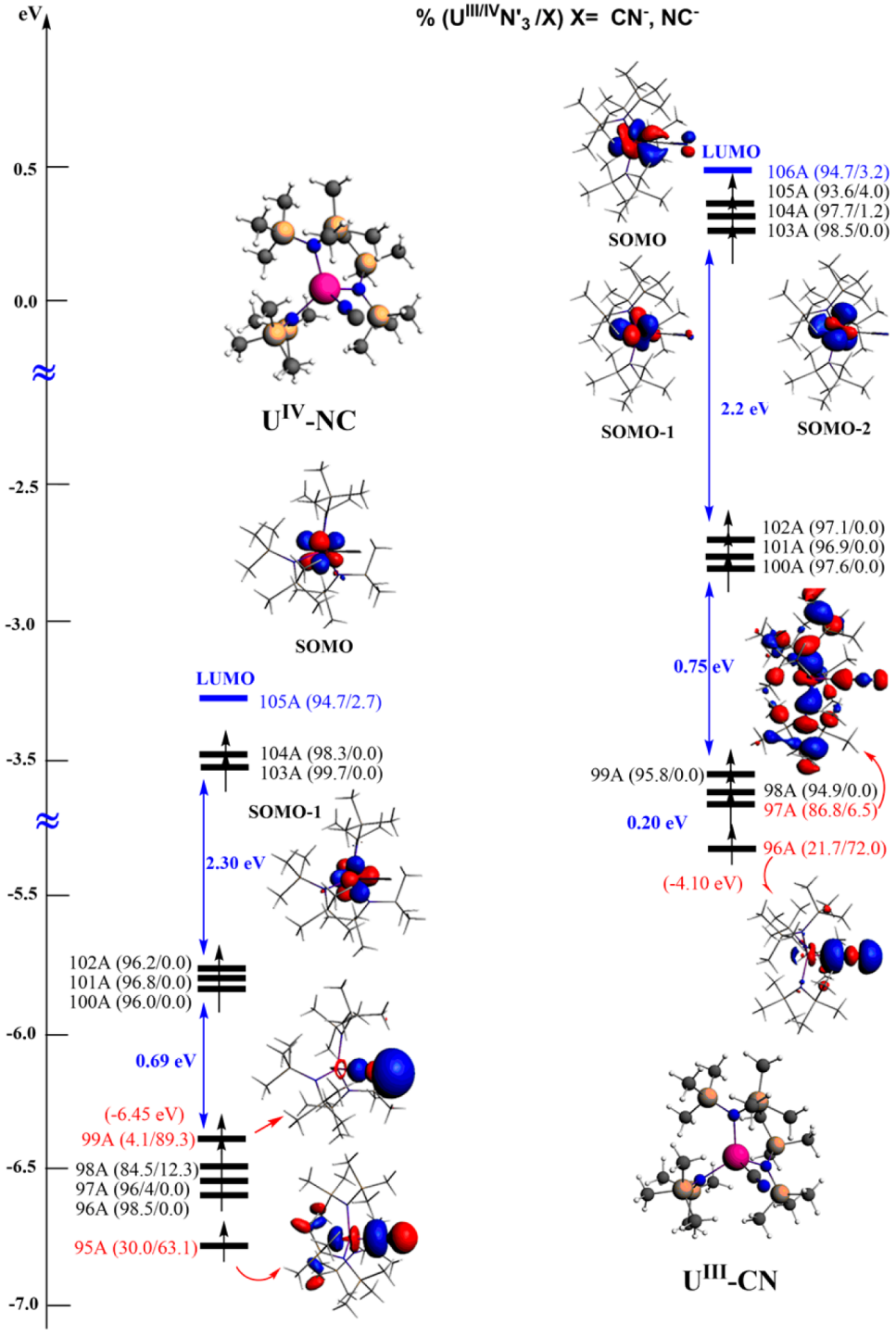

Figure 14. ZORA/BP86/TZP α-spin MO diagram for the complexes $[UN^*_3(CN)]^-$ and $[UN^*_3(NC)]$. Cutoff used, 0.03 e/bohr^3.

and H_c of the metallacycle U−CN bond are slightly larger than those in the isocyanide counterpart.

Molecular Orbital (MO) Analysis of the Mono-(cyanide/isocyanide) Complexes. To further assess the CN/NC coordination preference in the $[UN^*_3X]^q$ (q = 1−, 0) complexes, an interaction diagram between the $U^{III/IV}$ $[UN^*_3]^{0/+}$ and CN^- orbitals has been computed and is displayed in Figure 13. The better energy matching between the U^{III} $5f^3$ metallic fragment orbitals and the upper C-localized cyanide CN^- orbitals is in favor of U^{III}−CN coordination. Similarly, the deeper N-localized isocyanide NC^- orbitals interact more with U^{IV} $5f^2$ fragment orbitals, leading to the U^{IV}−NC coordination preference.

MO frontier diagrams of the $[UN^*_3X]^q$ (q = 1−, 0; X = CN/NC) complexes are presented in Figure 14. For the sake of simplicity, only the α-spin MOs are displayed; the U^{III}−CN and U^{IV}−NC MOs are shown on the right and left sides of the diagram, respectively. The percentages % (UN^*_3/X) represent the contributions of the $U^{III/IV}$ metallic fragment and the CN/NC ligands to the frontier MOs. As displayed in this diagram, two different but significant sets of MOs appear. For all complexes, the diagram shows that the highest occupied α-spin

DOI: 10.1021/acs.inorgchem.5b00034
Inorg. Chem. 2015, 54, 2474−2490

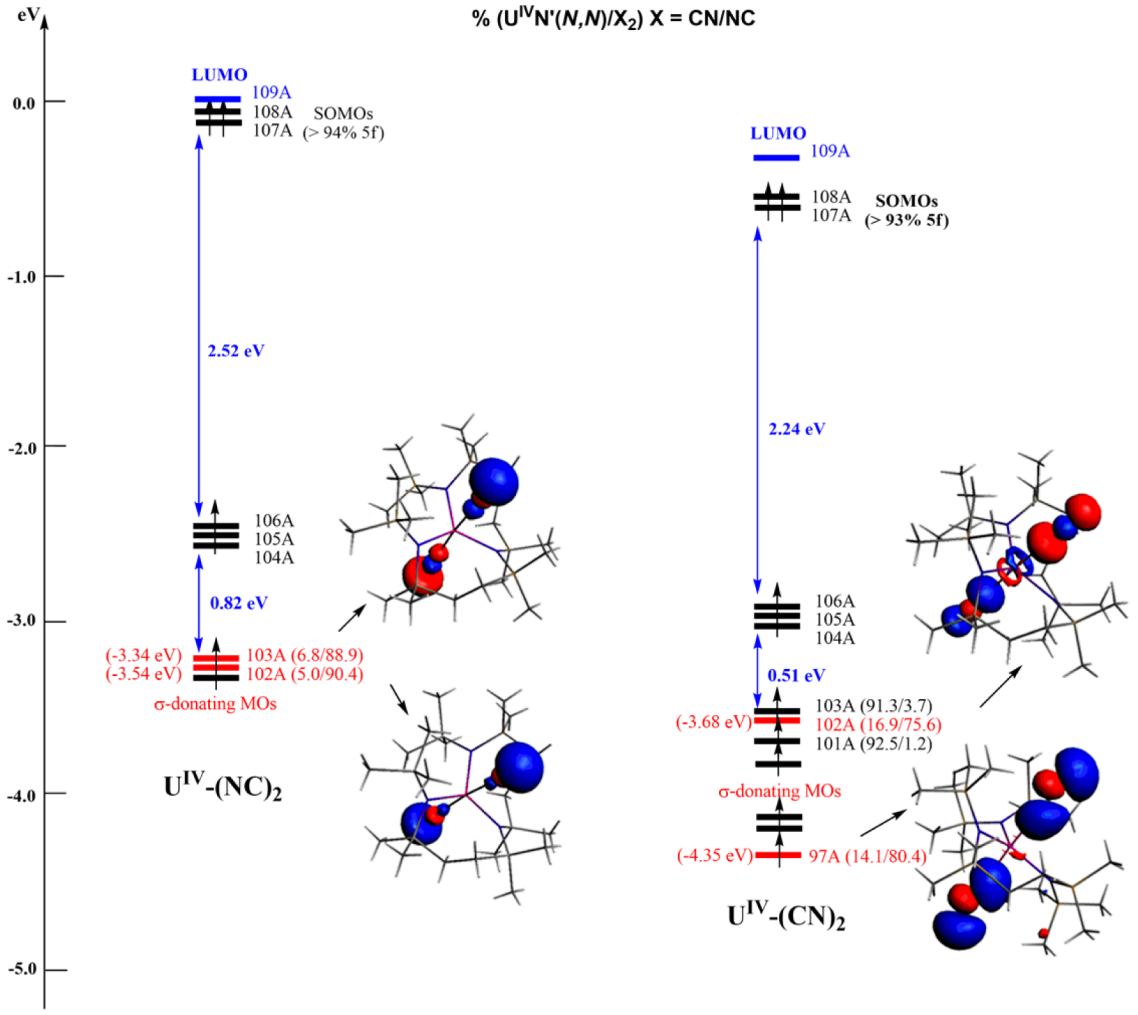

Figure 15. ZORA/BP86/TZP α-spin MO diagram for the metallacyclic complexes $[UN^*(N,N)X_2]^-$ (X = CN/NC). Cutoff used, 0.03 e/Bohr^3.

orbitals, i.e., SOMO, SOMO−1, and SOMO−2 of $[U^{III}N^*_3(CN)]^-$ $5f^3$ and SOMO and SOMO−1 of $[U^{IV}N^*_3(NC)]$ $5f^2$ complexes, are essentially metallic, with a dominant 5f orbital character. In line with QTAIM and NM analyses, a stronger U^{III}−CN bonding results from σ donation as shown by an important orbital mixing, namely, 72.0% of CN and 21.7% of $U^{III}N^*_3$ for MO 96A. Comparatively, the isocyanide U^{IV}−NC coordination is ensured by σ donation with an orbital mixing of 30% UN^*_3/63.1% NC for MO 95A and 4.1% UN^*_3/89.3% NC for MO 99A. It is also worth noting that the σ donation of MO 96A for U^{III}−CN cyanide bonding is located at a much higher energy (−4.10 eV) than its isocyanide U^{IV}−NC MOs 96A and 99A (∼−6.5 eV) counterparts, confirming the crucial energy matching rule for CN/NC coordination preference toward the U^{III}/U^{IV} pair, in good agreement with previous theoretical works.[1,47] As previously noted,[1] the $U^{III/IV}$−CN/NC coordination mode preference originates from both the σ-donating ability of ligands toward the $U^{III/IV}$ pair (best energy matching) and the orbital mixing (covalency) between the 6d/5f metal orbitals and the C-localized cyanide or N-localized isocyanide MO. We shall study below the stabilities of the actual cyanide and isocyanide systems.

Turning back to the metallacyclic $U^{IV}[UN^*(N,N)X_2]^-$ complex, we now consider the MO diagrams of the bis(cyanide/isocyanide) structures, depicted in Figure 15. The percentages $\%(UN(N,N)/X_2)$ represent the contributions of the U^{IV} metallic molecular fragment and the bis(CN/NC) ligands to the frontier MOs. The diagrams show that the highest occupied α-spin orbitals, i.e., the SOMOs for the triplet state ($5f^2$) complexes, are essentially metallic, with dominant 5f orbital character. Moreover, no metal-to-ligand π^* back-donation is observed in these frontier MOs. The main difference between the cyanide and isocyanide species is noted considering the occupied MOs relative to the σ donation of the ligands. Indeed, these levels are significantly lower in energy for the cyanide than for the isocyanide coordination, as exemplified with the σ-donation MOs 97A versus 102A energy levels (i.e., −4.35 vs −3.54 eV). This energy difference is certainly partly responsible for the preferred $U-(CN)_2$ coordination in the $[UN^*(N,N)X_2]^-$ complex. This can also be illustrated by the higher mixing orbital and the energy splitting of the two σ-donating MO levels, which is significantly larger for the cyanide complex than for the isocyanide complex.

Energy Decomposition Analysis. In order to investigate the energetic factors driving the cyanide/isocyanide coordination preference toward U^{III} and U^{IV} ions, the total bonding energies TBE_{frag} between the metal and cyanide ligand have been computed. Molecular fragments have been considered as follows:

DOI: 10.1021/acs.inorgchem.5b00034
Inorg. Chem. 2015, 54, 2474−2490

Table 8. Energy Decomposition Analysis at the ZORA/BP86/TZP Level for the Mono- and Bis(cyanide/isocyanide) Complexes $[UN^*_3X]^q$ (q = 1−, 0), $[UN^*_3X_2]^q$ (q = 2−, 1−) and $[UN^*(N,N)X_2]^-$ (X = CN, NC)

X = CN/NC	E_{st} (eV)	E_{orb}(eV)	TBE_{frag}(eV)	relative stability ΔE (kcal mol^{-1})
$U^{III}N^*_3$−X	+0.391/+0.038	−3.976/−3.246	−3.584/−3.208	0.0/8.7
$U^{IV}N^*_3$−X	−3.068/−3.134	−2.966/−3.469	−6.035/−6.603	13.1/0.0
$U^{III}N^*_3$−X_2[1]	+0.349/+0.517	−5.846/−5.630	−5.497/−5.112	0.0/8.9
$U^{IV}N^*_3$−X_2	−6.492/−6.103	−5.255/−5.715	−11.747/−11.817	1.6/0.0
$U^{IV}N^*(N,N)$−X_2	−6.582/−6.264	−5.089/−5.354	−11.671/−11.618	0.0/1.4

$$[UN^*_3]^{0/+} + X^- \rightarrow [UN^*_3UX]^q \quad (X = CN/NC;\ q = 1-, 0)$$

$$[UN^*_3]^{0/+} + 2X^- \rightarrow [UN^*_3UX_2]^q \quad (X = CN/NC;\ q = 2-, 1-)$$

TBE_{frag} values have been computed at the spin-unrestricted ZORA/BP86/TZP level (see the Computational Details). The results presented in Table 8 are in good agreement with the experimental findings, namely, that the complex exhibiting the highest TBE_{frag} is the most stable one. Indeed, considering the $[UN^*_3UX]^q$ (q = 1−, 0) complexes, it can be seen that TBE_{frag} for the U^{III}−CN coordination is larger (in absolute value) than that for the U^{III}−NC one (i.e., −3.584 vs −3.208 eV). The opposite is obtained for the U^{IV} complex, for which the most stable coordination is the U^{IV}−NC one (−6.035 vs −6.603 eV). Similarly, for the bis(cyanide/isocyanide) complexes $[UN^*_3UX_2]^q$ (q = 2−, 1−), our previous work[1] revealed that the cyanide U^{III}−CN coordination is more stable than the U^{III}−NC one (−5.497 vs −5.112 eV), whereas the opposite is obtained for the tetravalent U^{IV} complexes, where the U^{IV}−NC bonding is predicted to be slightly stronger than the U^{IV}−CN one (−11.747 vs −11.817 eV). The calculated TBE_{frag} values thus predict correctly the observed coordination.

We consider now the different energy terms, i.e., the steric E_{steric} and orbital E_{orb} energy terms composing TBE_{frag}: $TBE_{frag} = E_{steric} + E_{orb}$ (see the Computational Details). These two terms (Table 8) drive the CN/NC coordination preference toward the $U^{III/IV}$ pair. First, it is worth remembering that the orbital E_{orb} part includes both a polarization term due to the rearrangement of the metal and ligand charge distribution with complexation and some possible covalence if their orbitals overlap.[47g,i,j] Unfortunately, these two terms cannot be evaluated separately.[47i] Moreover, the repolarization component is likely not the same for the C or N coordination modes so that differences in E_{orb} cannot be directly related to differences in covalency. For the U^{III} mono(CN/NC) complexes, because the steric part of TBE is positively small, the U^{III}−CN coordination preference is largely favored by the E_{orb} term, which is more important (in absolute value) than that for the U^{III}−NC coordination (−3.976 vs −3.246 eV). In the same way, the U^{IV} case reveals a more negative E_{orb} term for U^{IV}−NC than for U^{IV}−CN (−3.469 vs −2.966 eV). On the other hand, the steric E_{steric} term, which is summed from the Pauli repulsion (repulsion between electron pairs) and stabilizing electrostatic interactions, shows that the cyanide/isocyanide U^{III}−CN/NC binding mode is sterically unfavorable compared to U^{IV}−CN/NC. The difference is due to the larger electrostatic term because of the differently charged $[N^*_3U]^{0/+}$ species, whereas Pauli repulsions do not vary significantly. It is also notable that, in the case of the U^{IV} monocoordination, the U^{IV}−NC bond distance is shorter than the U^{IV}−CN one, leading to a higher polarization effect for the isocyanide ligand and then to a more important effect on the orbital energies.[47i] This partly explains the significantly larger orbital term (in absolute value) for the NC versus CN coordination.

As previously stated,[1,42g,47d] the orbital term E_{orb} (stabilizing energy partly due to orbital mixing) correlates with TBE_{frag} satisfactorily in predicting the CN/NC coordination preference toward $U^{III/IV}$, except for the U^{IV} metallacyclic complex $[UN^*(N,N)(CN)_2]$. Interestingly, the comparison between the cyanide U^{III}−CN and isocyanide U^{IV}−NC coordination modes shows a decrease of the orbital term E_{orb} (−3.976 vs −3.469 eV). The fact that TBE_{frag} is significantly larger for U^{IV}−NC binding than for U^{III}−CN binding is mainly due to the higher stabilization provided by the negative steric term E_{steric}, namely, −3.134 versus 0.391 eV, respectively. The same conclusion can be drawn for the bis(cyanide/isocyanide) $[U^{III}N^*_3(CN)_2]^{2-}$ and $[U^{IV}N^*_3(NC)_2]^-$ complexes. Concerning the metallacyclic $[UN^*(N,N)(CN)_2]^-$ complex, which, in contrast to $[UN^*_3(NC)_2]^-$, exhibits the U−CN coordination mode, the energy difference between the actual cyanide and hypothetical isocyanide complexes is small. Looking at the energy decomposition, it can be seen that, although the computed orbital energy E_{orb} term is larger for U−NC coordination than for U−CN coordination (−5.354 vs −5.089), the E_{steric} term acts more importantly toward the observed U−CN coordination. Finally, we can conclude that the U−CN/NC coordination preference toward the U^{III}/U^{IV} pair is related to the subtle balance between steric, covalent, and ionic factors that govern U−CN/NC bonding. The energy decomposition calculations combined with QTAIM analysis indicated a predominantly ionic U−CN/NC bonding but also a significant contribution of the orbital interaction to the bonding. Theoretical investigation of triatomic cyanides M−CN and isocyanides M−NC of first-row transition metals already brought to light the delicate balance between electrostatic and orbital effects that drive the chosen coordination.[48] These subtle effects are also at work considering the Ti^{IV} complexes $[Ti(CN)_n]^{4-n}$ (n = 1−6), leading to the Ti−NC coordination for n = 1−5 and Ti−CN for n = 6.[49] It is also worth noting that NM bond orders correlate nicely with the observed U−CN/NC coordination preferences of the complexes under consideration. The computed TBE_{frag} allows in all cases to predict the observed coordination mode.

CONCLUSION

Uranium(IV) cyanide complexes in the tris(silylamide) UN^*_3 series could not be obtained by the oxidation of trivalent precursors but were easily isolated from addition reactions of CN^- to the cationic complex **1**, which was prepared by protonolysis of the metallacycle $[UN^*_2(N,C)]$ [N,C = $CH_2SiMe_2N(SiMe_3)$] with $[HNEt_3][BPh_4]$. The cyanido-bridged dinuclear compound **7** and the mononuclear mono-

DOI: 10.1021/acs.inorgchem.5b00034
Inorg. Chem. 2015, 54, 2474−2490

and bis(cyanide) complexes **2** and $[M][UN^*_3(CN)_2]$ [M = $K(THF)_4$ and K(18-crown-6)] were characterized by their X-ray crystal structure. In contrast to their U^{III} analogues $[NMe_4][UN^*_3(CN)]$ and $[K(18\text{-crown-6})]_2[UN^*_3(CN)_2]$ in which the CN anions are coordinated to the metal center via the C atom, the U^{IV} derivatives exhibit the isocyanide U−NC coordination mode of the cyanide ligand. The observed coordination preference of the cyanide and isocyanide ligands toward U^{III} and U^{IV} complexes has been computationally investigated. Consideration of the actual complexes and their hypothetical counterparts $[UN^*_3X]^q$ (q = 1−, 0) and $[UN^*_3X_2]^q$ (q = 2−, 1−) (X = CN, NC) shows that the stronger σ-donating ability of cyanide and isocyanide toward the U^{III}/U^{IV} pair is governed by the best energy matching between 6d/5f metal and ligand orbitals and covalency contribution (orbital mixing). This latter effect seems to play a more significant role for the observed U^{III}−CN coordination than for the U^{IV}−NC coordination. A comparison of the different quantum descriptors, i.e., bond orders, NPA/QTAIM data, and energy decomposition analysis, has allowed highlighting of the subtle balance between covalent, ionic, and steric factors that govern the U−CN/NC bonding. Furthermore, the U^{III}−CN versus U^{IV}−NC coordination mode observed in the tris(silylamide) UN^*_3 complexes cannot be considered as a general feature because the structure of the metallacyclic bis(cyanide) complex $[NEt_4][U^{IV}N^*(N,N)(CN)_2]$ revealed the U^{IV}−C ligation mode of the CN ligand. These distinct coordination modes remain difficult to explain because of the small energy difference between the cyanide and isocyanide complexes, but in all cases, DFT computations afforded good predictions of the observed U−CN/NC coordination preferences.

EXPERIMENTAL SECTION

General Procedure. All reactions were carried out under argon with the rigorous exclusion of air and water (<5 ppm oxygen or water) using standard Schlenk-vessel and vacuum-line techniques or in a glovebox. Solvents were thoroughly dried by standard methods and distilled immediately before use. The commercial reagents (Fluka, Aldrich) KCN, CuCN, $CuBr_2$, NEt_4CN, N^nBu_4CN, $[HNEt_3]Cl$, and pyridine-*N*-oxide have been used as received. [pyH][OTf] was precipitated by the addition of pyridine into a solution of TfOH in Et_2O, and $[HNEt_3][BPh_4]$ was obtained by mixing $[HNEt_3]Cl$ and $NaBPh_4$ in water. 18-crown-6 (Fluka) was dried under vacuum before use. $[UN^*_3]$,[50] $[UN^*_2(N,C)]$,[9] and $[K(18\text{-crown-6})][UN^*_3(CN)]$[1] were prepared according to literature procedures. IR samples were prepared as Nujol mulls between KBr round cell windows and the spectra recorded on a PerkinElmer FT-IR 1725X spectrometer. The ^1H and $^{13}C\{^1H\}$ NMR spectra were recorded on a 200 instrument at 20 °C when not otherwise specified and referenced internally using the residual protio solvent resonances relative to tetramethylsilane (δ 0). The signals corresponding to the CN ligands were not visible on the $^{13}C\{^1H\}$ NMR spectra. Elemental analyses were performed by Analytische Laboratorien at Lindlar (Germany) or by Medac Ltd. at Chobham (UK).

Reaction of $[UN^*_3]$ and CuCN. An NMR tube was charged with $[UN^*_3]$ (10.0 mg, 0.014 mmol) and CuCN (6.25 mg, 0.07 mmol) in benzene-d_6 (0.5 mL). After 48 h at 20 °C, the spectrum of the brown solution showed the presence of $[UN^*_2(N,C)]$ as the sole uranium product.

Reaction of $[UN^*_3(Cl)]$ (3) and NEt_4CN. An NMR tube was charged with **3** (20.0 mg, 0.027 mmol) and NEt_4CN (13.46 mg, 0.053 mmol) in THF-d_8 (0.5 mL). The tube was immersed in an ultrasound bath, and after 24 h, the spectrum of the pale-brown solution showed a large signal of the N* ligands at δ −3.16 ($w_{1/2}$ ∼ 700 Hz). Cooling the THF solution led to the formation of pale-pink platelets of $[NEt_4][UN^*_3(Cl)(CN)]$, whose structure could not be determined with accuracy because of their poor quality for X-ray diffraction analysis.

Synthesis of $[UN^*_3][BPh_4]$ (1). A 50 mL flask was charged with $[UN^*_2(N,C)]$ (1000 mg, 1.4 mmol) and $[HNEt_3][BPh_4]$ (578 mg, 1.37 mmol), and THF (20 mL) was distilled in it under reduced pressure at −78 °C. After stirring for 30 min, the pale-brown solution was evaporated to dryness, and the beige powder of **1** was washed with toluene (20 mL) and pentane (2 × 15 mL) and dried under vacuum (1300 mg, 86%). Anal. Calcd for $C_{42}H_{74}BN_3Si_6U$: C, 48.58; H, 7.18; N, 4.05. Found: C, 48.94; H, 7.03; N, 3.65. ^1H NMR (THF-d_8): δ_H 5.49 (t, J = 7.1 Hz, 4H, *p*-Ph), 5.20 (t, J = 7.1 Hz, 8H, *m*-Ph), 4.80 (m, 8H, *o*-Ph), −3,54 (s, 54H, $SiMe_3$). ^1H NMR (pyridine-d_5): δ_H 7.44 (m, 8H, Ph), 6.78 (m, 12H, Ph), −3.98 (s, 54H, $SiMe_3$). ^1H NMR (benzene-d_6): δ_H 2.91 (m, 4H, *p*-Ph), 2.82 (m, 8H, Ph), 1.60 (m, 8H, BPh_4), −6.33 (s, 54H, $SiMe_3$). $^{13}C\{^1H\}$ NMR (THF-d_8): δ_C 162.9 (q, J_{C-B} = 49.4 Hz, *ipso*-Ph), 133.8 (Ph), 124.1 (q, J_{C-B} = 2.7 Hz, *o*-Ph), 119.4 (Ph), −4.7 ($SiMe_3$). $^{13}C\{^1H\}$ NMR (benzene-d_6): δ_C 130.5 (Ph), 120.4 (Ph), 116.7 (Ph), −6.1 ($SiMe_3$). The signal of the *ipso*-C atoms is not visible. Pale-green platelets of **1**(THF) were obtained by the slow diffusion of Et_2O into a THF solution of **1**.

Synthesis of $[UN^*_3(CN)]$ (2). A 50 mL flask was charged with **1** (300 mg, 0.29 mmol) and NEt_4CN (42.8 mg, 0.26 mmol), and THF (20 mL) was distilled in it under reduced pressure at −78 °C. After stirring for 15 h at 20 °C, precipitation of $[NEt_4][BPh_4]$ was observed. The solvent was evaporated off, and **2** was extracted in Et_2O by Soxhlet extraction and isolated as a pink powder after drying under vacuum (145 mg, 75%). Anal. Calcd for $C_{19}H_{54}N_4Si_6U$: C, 30.62; H, 7.30; N, 7.51. Found: C, 30.66; H, 7.27; N, 7.50. ^1H NMR (THF-d_8): δ_H −3.07 (s, $w_{1/2}$ = 49 Hz, 54H, $SiMe_3$). ^1H NMR (benzene-d_6): δ_H −2.81 (s, $w_{1/2}$ = 83 Hz, 54H, $SiMe_3$). $^{13}C\{^1H\}$ NMR (THF-d_8): δ_C −13.6 ($SiMe_3$). $^{13}C\{^1H\}$ NMR (benzene-d_6): δ_C −14.5 ($SiMe_3$). IR (Nujol): ν(CN) 2044 cm^{-1}. Pale-pink crystals of **2** were obtained by crystallization from a 1:5 mixture of pentane and THF at −35 °C.

Synthesis of $[UN^*_3(Cl)]$ (3). An NMR tube was charged with $[UN^*_2(N,C)]$ (20.0 mg, 0.028 mmol) and $[HNEt_3][Cl]$ (3.99 mg, 0.028 mmol) in THF-d_8 (0.5 mL). After 24 h at 20 °C, the spectrum showed the complete conversion of the metallacycle into **3**, characterized by a singlet at δ −2.48. The solvent was evaporated off, and pentane (0.5 mL) was added. Cooling the solution at −35 °C led to the formation of brown crystals of **3**.

Synthesis of $[UN^*_3(OTf)]$ (4). (a) A 50 mL flask was charged with $[UN^*_2(N,C)]$ (310 mg, 0.43 mmol) and [pyH][OTf] (98.5 mg, 0.43 mmol), and THF (20 mL) was distilled in it under reduced pressure at −78 °C. After stirring for 2 h at 20 °C, the pale-brown solution was evaporated to dryness, leaving the pale-brown powder of **4**, which was washed with pentane (20 mL) and then Et_2O (20 mL) and dried under vacuum (321 mg, 86%). Anal. Calcd for $C_{19}H_{54}F_3N_3O_3SSi_6U$: C, 26.28; H, 6.27; N, 4.84. Found: C, 26.66; H, 5.93; N, 4.76. ^1H NMR (THF-d_8): δ_H −1.45 (s, 54 H, $SiMe_3$). ^1H NMR (benzene-d_6): δ_H −1.34 (s, 54 H, $SiMe_3$). $^{13}C\{^1H\}$ NMR (THF-d_8): δ_C −5.0 ($SiMe_3$). $^{13}C\{^1H\}$ NMR (benzene-d_6): δ_C −4.9 ($SiMe_3$). IR (Nujol): 1196, 1162, 992 cm^{-1}. Pinkish crystals of **4** were formed at −35 °C by crystallization in a pentane−THF mixture.

(b) An NMR tube was charged with $[U(N^*)_3]$ (10.0 mg, 0.014 mmol) and Ph_3COTf (5.48 mg, 0.014 mmol) in benzene-d_6 (0.5 mL). The violet color of the solution turned immediately orange, and the spectrum showed the formation of **4** as the sole uranium complex (δ_H −1.34) and of Gomberg's dimer $Ph_3CCH(C_4H_4)C{=}CPh_2$.

Synthesis and Crystals of $[\{UN^*(\mu\text{-}N,C)(\mu\text{-}OTf)\}_2]$ (5) and $[\{UN^*(N,C)(THF)(\mu\text{-}OTf)\}_2]$ (6). A 50 mL flask was charged with **4** (124.5 mg, 0.14 mmol), and THF (20 mL) was distilled in it under reduced pressure at −78 °C. After stirring for 2 days at 70 °C, the brown solution was evaporated to dryness, leaving a brown powder that was crystallized in Et_2O (5 mL) at −33 °C. The brown crystals of **5** were filtered off and dried under vacuum (42.5 mg, 42%). Anal. Calcd for $C_{26}H_{70}F_6N_4O_6S_2Si_6U_2$: C, 23.00; H, 5.20; N, 4.13. Found: C, 22.25; H, 4.87; N, 4.01. ^1H NMR (THF-d_8): δ_H 35.03 (s, 18H, $SiMe_3$), 15.84 (s, 12H, $SiMe_2$), −0.72 (s, 36H, $SiMe_3$), −228.72 (s, 4H, CH_2). ^1H NMR (benzene-d_6): δ_H 34.48 (s, 12H, $SiMe_2$), 17.37 (s, 18H,

DOI: 10.1021/acs.inorgchem.5b00034
Inorg. Chem. 2015, 54, 2474−2490

Table 9. Crystal Data and Structure Refinement Details

	1(THF)	2	3	4	5
chemical formula	$C_{50}H_{90}BN_3O_2Si_6U$	$C_{19}H_{54}N_4Si_6U$	$C_{18}H_{54}ClN_3Si_6U$	$C_{19}H_{54}F_3N_3O_3SSi_6U$	$C_{26}H_{70}F_6N_4O_6S_2Si_8U_2$
M (g mol^{-1})	1182.63	745.23	754.66	868.28	1413.76
cryst syst	triclinic	trigonal	trigonal	triclinic	triclinic
space group	$P\bar{1}$	$R3c$	$R3c$	$P\bar{1}$	$P\bar{1}$
a (Å)	16.9269(7)	18.4684(6)	18.4359(3)	11.9323(5)	11.2771(6)
b (Å)	18.7867(6)	18.4684(6)	18.4359(3)	12.1577(8)	11.4316(5)
c (Å)	19.4285(7)	16.9719(10)	16.9152(4)	12.7144(8)	11.6871(7)
α (deg)	107.7551(18)	90	90	87.839(3)	80.495(3)
β (deg)	93.7460(18)	90	90	87.957(4)	88.841(2)
γ (deg)	91.4929(19)	120	120	89.746(4)	62.631(3)
V (Å^3)	5864.5(4)	5013.3(5)	4978.9(2)	1841.98(18)	1316.96(13)
Z	4	6	6	2	1
D_{calcd} (g cm^{-3})	1.339	1.481	1.510	1.566	1.783
μ(Mo Kα) (mm^{-1})	2.928	5.085	5.198	4.697	6.460
F(000)	2432	2232	2256	864	684
reflns collcd	348431	42748	40042	102157	69151
indep reflns	35783	3391	3370	11241	8033
obsd reflns [$I > 2\sigma(I)$]	24518	2255	2885	9896	6809
R_{int}	0.049	0.047	0.018	0.038	0.064
params refined	1169	98	95	342	255
R1	0.034	0.038	0.028	0.027	0.031
wR2	0.072	0.079	0.074	0.066	0.067
S	0.947	0.936	1.064	0.993	0.984
$\Delta\rho_{min}$ (e Å^{-3})	−1.15	−1.24	−0.86	−1.30	−1.46
$\Delta\rho_{max}$ (e Å^{-3})	0.65	2.05	0.45	0.88	1.50

	6	7·0.5Et$_2$O	9	10
chemical formula	$C_{34}H_{86}F_6N_4O_8S_2Si_8U_2$	$C_{63}H_{133}BN_7O_{0.5}Si_{12}U_2$	$C_{36}H_{86}KN_5O_4Si_6U$	$C_{32}H_{78}KN_5O_6Si_6U$
M (g mol^{-1})	1557.97	1820.71	1098.77	1074.66
cryst syst	triclinic	triclinic	monoclinic	monoclinic
space group	$P\bar{1}$	$P\bar{1}$	$C2/c$	$P2_1$
a (Å)	11.8587(10)	15.5570(10)	19.4829(10)	11.4734(9)
b (Å)	11.9910(10)	16.0199(10)	11.9358(7)	18.469(2)
c (Å)	12.5171(9)	19.1374(17)	24.8150(9)	13.0501(14)
α (deg)	92.187(5)	81.057(5)	90	90
β (deg)	104.462(5)	89.273(5)	108.710(3)	110.476(7)
γ (deg)	114.001(4)	67.531(4)	90	90
V (Å^3)	1554.7(2)	4348.1(5)	5465.6(5)	2590.6(5)
Z	1	2	4	2
D_{calcd} (g cm^{-3})	1.664	1.391	1.335	1.378
μ(Mo Kα) (mm^{-1})	5.482	3.923	3.213	3.391
F(000)	764	1842	2256	1096
reflns collcd	85800	191955	101389	109242
indep reflns	5913	16485	8338	9801
obsd reflns [$I > 2\sigma(I)$]	5280	11815	6050	8022
R_{int}	0.045	0.060	0.042	0.057
params refined	300	827	251	571
R1	0.048	0.051	0.044	0.058
wR2	0.128	0.114	0.107	0.142
S	1.089	1.027	1.007	1.048
$\Delta\rho_{min}$ (e Å^{-3})	−1.49	−2.07	−1.08	−1.53
$\Delta\rho_{max}$ (e Å^{-3})	3.10	1.75	1.17	1.48

$SiMe_3$), −18.08 (s, 36 H, $SiMe_3$), −520.11 (s, 4H, CH_2). Yellow platelets of **6** were obtained by crystallization of **5** from THF.

Synthesis of [(UN*$_3$)$_2$(μ-CN)][BPh$_4$] (7). A 50 mL flask was charged with **1** (150 mg, 0.14 mmol) and NEt_4CN (10.70 mg, 0.065 mmol), and THF (15 mL) was distilled in it under reduced pressure at −78 °C. After stirring for 15 h at 20 °C, the yellow solution was filtered and evaporated to dryness. The yellow solid was extracted in Et_2O (15 mL), and after evaporation of the solvent, the yellow powder of **7** was washed with pentane (2 × 20 mL) and dried under vacuum (74 mg, 65%). Anal. Calcd for $C_{61}H_{128}BN_7Si_{12}U_2$: C, 41.08; H, 7.23; N, 5.49. Found: C, 39.00; H, 6.50; N, 4.72. ^{1}H NMR (THF-d_8): δ_H 6.90, 6.66, 6.63 (m, 20H, BPh_4), −6.75 (s, $w_{1/2}$ = 74 Hz, 108H, $SiMe_3$). $^{13}C\{^1H\}$ NMR (THF-d_8): δ_C 165.0 (q, J_{C-B} = 50.2 Hz, *ipso*-Ph), 137.0 (*o*-Ph), 125.5 (*m*-Ph), 121.6 (*p*-Ph), −9.2 ($SiMe_3$). IR (Nujol): ν(CN) 2115 cm^{-1}. Yellow crystals of 7·0.5Et_2O were obtained by crystallization of **7** from Et_2O at −33 °C.

Synthesis of [NEt$_4$][UN*$_3$(CN)$_2$] (8). A 50 mL flask was charged with **1** (307 mg, 0.30 mmol) and NEt_4CN (97 mg, 0.60 mmol), and

DOI: 10.1021/acs.inorgchem.5b00034
Inorg. Chem. 2015, 54, 2474−2490

THF (15 mL) was distilled in it under reduced pressure at −78 °C. After stirring for 3 h at 20 °C, a white precipitate of $[NEt_4][BPh_4]$ was formed, and the pinkish solution was filtered and evaporated to dryness, leaving a pale-pink powder. Complex **8** was extracted in a 1:5 mixture of THF and Et_2O (15 mL) and isolated as a pink powder after evaporation of the solution and drying under vacuum (156 mg, 58%). Anal. Calcd for $C_{28}H_{74}N_6Si_6U$: C, 37.31; H, 8.27; N, 9.32. Found: C, 37.02; H, 8.21; N, 9.63. ^{1}H NMR (THF-d_8): δ_H 1.56 (s, 8H, NCH_2CH_3), −0.16 (s, 12H, NCH_2CH_3), −1.40 (br s, $w_{1/2}$ = 193 Hz, 54H, $SiMe_3$). ^{1}H NMR (pyridine-d_5): δ_H 2.07 (q, J = 7.2 Hz, 8H, NCH_2CH_3), 0.21 (t, J = 7.2 Hz, 12H, NCH_2CH_3), −0.39 (br s, $w_{1/2}$ ∼ 200 Hz, 54H, $SiMe_3$). $^{13}C\{^1H\}$ NMR (THF-d_8): δ_C 50.7 (s, NCH_2CH_3), 5.6 (s, NCH_2CH_3), −17.7 (s, $SiMe_3$). IR (Nujol): ν(CN) 2058 cm^{-1}.

Synthesis of K[UN*$_3$(CN)$_2$] and Crystals of [K(THF)$_4$][UN*$_3$(CN)$_2$] (9). A 50 mL flask was charged with **1** (500 mg, 0.48 mmol) and KCN (313.5 mg, 4.8 mmol), and THF (15 mL) was distilled in it under reduced pressure at −78 °C. After stirring for 15 h at 20 °C, the yellow reaction mixture was filtered, and the solvent was evaporated off to give a pale-green powder. Extraction in a 1:5 mixture of THF and Et_2O (15 mL), followed by evaporation to dryness, afforded a pale-green powder, which was recrystallized from THF to give pale-green crystals of **9**. The latter were transformed into $K[UN^*_3(CN)_2]$ upon drying under vacuum (243 mg, 63%). Anal. Calcd for $C_{20}H_{54}KN_5Si_6U$: C, 29.64; H, 6.72; N, 8.64. Found: C, 30.91; H, 6.88; N, 7.67. ^{1}H NMR (THF-d_8): δ_H −0.47 (br s, $w_{1/2}$ = 186 Hz, 54H, $SiMe_3$). ^{1}H NMR (pyridine-d_5): δ_H 0.32 (br s, $w_{1/2}$ = 184 Hz, 54H, $SiMe_3$). IR (Nujol): ν(CN) 2078 cm^{-1}.

Formation of [UN*$_3$(Br)$_2$] by Oxidation of 9 with CuBr$_2$. An NMR tube was charged with $K[UN^*_3(CN)_2]$ (10.0 mg, 0.012 mmol) and $CuBr_2$ (3.60 mg, 0.016 mmol) in THF-d_8 (0.5 mL). After 30 min at 20 °C, the spectrum of the red solution showed the signals of $[U(N^*)_3(Br)_2]$, and red crystals of this compound suitable for X-ray diffraction were formed upon cooling of the solution at −33 °C.[34]

Crystals of [K(18-crown-6)][UN*$_3$(CN)$_2$] (10). An NMR tube was charged with $[UN^*_3]$ (20.0 mg, 0.028 mmol), KCN (9.40 mg, 0.14 mmol), and 18-crown-6 (7.39 mg, 0.028 mmol) in Et_2O (0.5 mL). The tube was immersed in an ultrasound bath for 6 h, and pyridine *N*-oxide (2.66 mg, 0.028 mmol) was added to the dark-blue solution of $[K(18\text{-crown-6})][UN^*_3(CN)]$,[1] which immediately turned brown. After 1 h at 20 °C, the brown precipitate in the red solution was filtered off, and recrystallization in a 1:1 mixture of THF and Et_2O afforded pink crystals of **10** suitable for X-ray diffraction.

Crystallography. The data were collected at 150(2) K with a Nonius Kappa CCD area detector diffractometer[51] using graphite-monochromated Mo Kα radiation (λ = 0.71073 Å). The crystals were introduced into glass capillaries with a protective coating of Paratone-N oil (Hampton Research). The unit cell parameters were determined from 10 frames and then refined on all data. The data (combinations of φ and ω scans with a minimum redundancy of 4 for 90% of the reflections) were processed with *HKL2000*.[52] Absorption effects were corrected empirically with the program *SCALEPACK*.[52] The structures were solved by direct methods, expanded by subsequent difference Fourier synthesis, and refined by full-matrix least squares on F^2 with *SHELXL-97*.[53] All non-H atoms were refined with anisotropic displacement parameters. In the case of compounds **2** and **9**, it has been possible to determine unambiguously the location of the C and N atoms by selecting the solution giving the most satisfying refined displacement parameters (i.e., close to one another for a bridging cyanide or giving the most regular progression from metal to terminal atom for a monodentate cyanide). In compounds **7** and **10**, mixing of the two cyanide orientations was considered (see below). The H atoms were introduced at calculated positions (except for those bound to C1 in **5**, which were found on a difference Fourier map) and treated as riding atoms with an isotropic displacement parameter equal to 1.2 times that of the parent atom (1.5 for CH_3, with optimized geometry). Special details are as follows:

7·0.5Et_2O. The cyanide ligand is disordered over the two possible positions, which were given occupancy factors of 0.5 and refined with constraints on coordinates and displacement parameters. The Et_2O solvent molecule is disordered around an inversion center, and it has been refined with an occupancy factor of 0.5 and restraints on the bond lengths and displacement parameters.

10. The three N* ligands are disordered over two positions each, with N atoms common to both positions and also some common C atoms. These two sets of positions correspond to the two orientations of the helical arrangement, and they were given occupancy factors of 0.5. The exact location of the C and N atoms in the cyanide/isocyanide anions cannot be determined from the values of the displacement parameters, and both sites were refined with a mixture of C and N, with a refined occupancy factor and constraints on coordinates and displacement parameters. With the quality of the data being quite low, many restraints were necessary, particularly in the disordered parts.

Crystal data and structure refinement parameters are given in Table 9. The molecular plots were drawn with *ORTEP-3*.[54]

Computational Details. The methods and procedures were described in our previous paper on U−CN versus Ce−NC coordination in trivalent complexes derived from MN^*_3 (M = Ce, U).[1]

■ ASSOCIATED CONTENT

Supporting Information

Tables of crystal data, atomic positions, and displacement parameters, anisotropic displacement parameters, and bond lengths and bond angles in CIF format, as well as DFT-optimized geometries. This material is available free of charge via the Internet at http://pubs.acs.org.

■ AUTHOR INFORMATION

Corresponding Authors

*E-mail: jean-claude.berthet@cea.fr.
*E-mail: lotfi.belkhiri@umc.edu.dz.
*E-mail: abdou.boucekkine@univ-rennes1.fr.
*E-mail: michel.ephritikhine@cea.fr.

Notes

The authors declare no competing financial interest.

■ ACKNOWLEDGMENTS

The authors are grateful to GENCI-IDRIS and GENCI-CINES for an allocation of computing time (Grant 2013/2014-080649).

■ REFERENCES

(1) Hervé, A.; Bouzidi, Y.; Berthet, J. C.; Belkhiri, L.; Thuéry, P.; Boucekkine, A.; Ephritikhine, M. *Inorg. Chem.* **2014**, *53*, 6995.

(2) (a) Bradley, D. C.; Chisholm, M. H. *Acc. Chem. Res.* **1976**, *9*, 273. (b) Lappert, M. F.; Power, P. P.; Sanger, A. R.; Srivastava, R. C. C. *Metal and Metalloid Amides*; Ellis Horwood: Chichester, England, 1980. (c) Edelmann, F. In *Comprehensive Organometallic Chemistry*; Abel, E. W., Stone, F. G. A., Wilkinson, G., Eds.; Pergamon: Oxford, U.K., 1995; Vol. 4, Chapter 2, p 11. (d) Burns, C. J.; Eisen, M. S. In *The Chemistry of the Actinides and Transactinide Elements*; Morss, L. R., Edelstein, N. M., Fuger, J., Eds.; Springer: Dordrecht, The Netherlands, 2006; Vol. 5, Chapter 25, p 2799. (e) Lappert, M. F.; Protchenko, A. V.; Power, P. P.; Seeber, A. L. *Metal Amide Chemistry*; Wiley: Chichester, England, 2009.

(3) Thomson, R. K.; Graves, C. R.; Scott, B. L.; Kiplinger, J. L. *Inorg. Chem. Commun.* **2011**, *14*, 1742.

(4) (a) Simpson, S. J.; Turner, H. W.; Andersen, R. A. *Inorg. Chem.* **1981**, *20*, 2991. (b) Karl, M.; Harms, K.; Seybert, G.; Massa, W.; Fau, S.; Frenking, G.; Dehnicke, K. *Z. Anorg. Allg. Chem.* **1999**, *625*, 2055. (c) Han, F.; Zhang, J.; Yi, W.; Zhang, Z.; Yu, J.; Weng, L.; Zhou, X. *Inorg. Chem.* **2010**, *49*, 2793.

(5) Bénaud, O.; Berthet, J. C.; Thuéry, P.; Ephritikhine, M. *Inorg. Chem.* **2010**, *49*, 8117.

DOI: 10.1021/acs.inorgchem.5b00034
Inorg. Chem. 2015, 54, 2474−2490

(6) Bénaud, O.; Berthet, J.-C.; Thuéry, P.; Ephritikhine, M. *Inorg. Chem.* **2011**, *50*, 12204.
(7) Maynadié, J.; Berthet, J. C.; Thuéry, P.; Ephritikhine, M. *Organometallics* **2007**, *26*, 4585.
(8) Lewis, A. J.; Williams, U. J.; Carroll, P. J.; Schelter, E. J. *Inorg. Chem.* **2013**, *52*, 7326.
(9) Dormond, A.; El Bouadili, A.; Aaliti, A.; Moise, C. *J. Organomet. Chem.* **1985**, *288*, C1.
(10) Berthet, J. C.; Boisson, C.; Lance, M.; Vigner, J.; Nierlich, M.; Ephritikhine, M. *J. Chem. Soc., Dalton Trans.* **1995**, 3019.
(11) Evans, W. J.; Nyce, G. W.; Forrestal, K. J.; Ziller, J. W. *Organometallics* **2002**, *21*, 1050.
(12) (a) Gomberg, M. *Ber. Dtsch. Chem. Ges.* **1900**, *33*, 3150. (b) Lankamp, H.; Nauta, W. T.; MacLean, C. *Tetrahedron Lett.* **1968**, *9*, 249.
(13) Arnold, P. L.; Turner, Z. R.; Kaltsoyannis, N.; Pelekanaki, P.; Bellabarba, R. M.; Tooze, R. P. *Chem.—Eur. J.* **2010**, *16*, 9623.
(14) Berthet, J. C.; Nierlich, M.; Ephritikhine, M. *Eur. J. Inorg. Chem.* **2002**, *2002*, 850.
(15) Turner, H. W.; Andersen, R. A.; Zalkin, A.; Templeton, D. H. *Inorg. Chem.* **1979**, *18*, 1221.
(16) (a) Williams, U. J.; Robinson, J. R.; Lewis, A. J.; Carroll, P. J.; Walsh, P. J.; Schelter, E. J. *Inorg. Chem.* **2014**, *53*, 27. (b) Stewart, J. L. *Tris[bis(trimethylsilyl)amido]uranium: Compounds with Tri-, Tetra-, and Pentavalent Uranium*; Lawrence Berkeley Laboratory: Berkeley, CA, 1988.
(17) Fortier, S.; Brown, J. L.; Kaltsoyannis, N.; Wu, G.; Hayton, T. W. *Inorg. Chem.* **2012**, *51*, 1625.
(18) Hitchcock, P. B.; Hulkes, A. G.; Lappert, M. F. *Inorg. Chem.* **2004**, *43*, 1031.
(19) Airoldi, C.; Bradley, D. C.; Chudzynska, H.; Hursthouse, M. B.; Abdul Malik, K. M.; Raithby, P. R. *J. Chem. Soc., Dalton Trans.* **1980**, 2010.
(20) Williams, U. J.; Carroll, P. J.; Schelter, E. J. *Inorg. Chem.* **2014**, *53*, 6338.
(21) Nakai, H.; Hu, X.; Zakharov, L. N.; Rheingold, A. L.; Meyer, K. *Inorg. Chem.* **2004**, *43*, 855.
(22) Shannon, R. D. *Acta Crystallogr., Sect. A* **1976**, *32*, 751.
(23) Ren, W.; Zi, G.; Fang, D.-C.; Walter, M. D. *J. Am. Chem. Soc.* **2011**, *133*, 13183.
(24) Zi, G.; Jia, L.; Werkema, E. L.; Walter, M. D.; Gottfriedsen, J. P.; Andersen, R. A. *Organometallics* **2005**, *24*, 4251.
(25) Natrajan, L.; Mazzanti, M.; Bezombes, J.-P.; Pécaut, J. *Inorg. Chem.* **2005**, *44*, 6115.
(26) Evans, W. J.; Takase, M. K.; Ziller, J. W.; Rheingold, A. L. *Organometallics* **2009**, *28*, 5802.
(27) Kiplinger, J. L.; John, K. D.; Morris, D. E.; Scott, B. L.; Burns, C. J. *Organometallics* **2002**, *21*, 4306.
(28) Evans, W. J.; Walensky, J. R.; Furche, F.; Ziller, J. W.; DiPasquale, A. G.; Rheingold, A. L. *Inorg. Chem.* **2008**, *47*, 10169.
(29) Korobkov, I.; Gambarotta, S. *Inorg. Chem.* **2010**, *49*, 3409.
(30) Niemeyer, M. *Inorg. Chem.* **2006**, *45*, 9085.
(31) Yu, X.; Bi, S.; Guzei, I. A.; Lin, Z.; Xue, Z.-L. *Inorg. Chem.* **2004**, *43*, 7111.
(32) Berno, P.; Minhas, R.; Hao, S.; Gambarotta, S. *Organometallics* **1994**, *13*, 1052.
(33) Messere, R.; Spirlet, M. R.; Jan, D.; Demonceau, A.; Noels, A. F. *Eur. J. Inorg. Chem.* **2000**, 1151.
(34) Lewis, A. J.; Nakamaru-Ogiso, E.; Kikkawa, J. M.; Carroll, P. J.; Schelter, E. J. *Chem. Commun.* **2012**, *48*, 4977.
(35) Lewis, A. J.; Mullane, K. C.; Nakamaru-Ogiso, E.; Carroll, P. J.; Schelter, E. J. *Inorg. Chem.* **2014**, *53*, 6944.
(36) Maynadié, J.; Barros, N.; Berthet, J. C.; Thuéry, P.; Maron, L.; Ephritikhine, M. *Angew. Chem., Int. Ed.* **2007**, *46*, 2010.
(37) Berthet, J. C.; Thuéry, P.; Ephritikhine, M. *Organometallics* **2008**, *27*, 1664.
(38) Hervé, A.; Thuéry, P.; Ephritikhine, M.; Berthet, J.-C. *Organometallics* **2014**, *33*, 2088.
(39) Maynadié, J.; Berthet, J. C.; Thuéry, P.; Ephritikhine, M. *Organometallics* **2007**, *26*, 2623.
(40) Berthet, J.-C.; Thuéry, P.; Ephritikhine, M. *Chem. Commun.* **2007**, 604.
(41) (a) Wu, Q. Y.; Wang, C. Z.; Lan, J. H.; Xiao, C. L.; Wang, X. K.; Zhao, Y. L.; Chai, Z. F.; Shi, W. Q. *Inorg. Chem.* **2014**, *53*, 9607. (b) Averkiev, B.; Mantina, M.; Valero, R.; Infante, I.; Kovacs, A.; Truhlar, D.; Gagliardi, L. *Theor. Chem. Acc.* **2011**, *129*, 657.
(42) (a) Roger, M.; Belkhiri, L.; Arliguie, T.; Thuéry, P.; Boucekkine, A.; Ephritikhine, M. *Organometallics* **2008**, *27*, 33. (b) Gaunt, A. J.; Reilly, S. D.; Enriquez, A. E.; Scott, B. L.; Ibers, J. A.; Sekar, P.; Ingram, K. I. M.; Kaltsoyannis, N.; Neu, M. P. *Inorg. Chem.* **2008**, *47*, 29. (c) Gaunt, A. J.; Reilly, S. D.; Enriquez, A. E.; Scott, B. J.; Ibers, J. A.; Sekar, P.; Ingram, K. I. M.; Kaltsoyannis, N.; Neu, M. P. *Inorg. Chem.* **2008**, *47*, 29. (d) Roger, M.; Belkhiri, L.; Thuéry, P.; Bouaoud, S. E.; Boucekkine, A.; Ephritikhine, M. *Inorg. Chem.* **2009**, *48*, 221. (e) Meskaldji, S.; Belkhiri, L.; Arliguie, T.; Fourmigué, M.; Ephritikhine, M.; Boucekkine, A. *Inorg. Chem.* **2010**, *49*, 3192. (f) Meskaldji, S.; Zaiter, A.; Belkhiri, L.; Boucekkine, A. *Theor. Chem. Acc.* **2012**, *131*, 1151. (g) Zaiter, A.; Boudersa, A.; Bouzidi, Y.; Meskaldji, S.; Belkhiri, L.; Boucekkine, A.; Ephritikhine, M. *Inorg. Chem.* **2014**, *53*, 4687−4697.
(43) (a) Sonnenberg, J. L.; Hay, P. J.; Martin, R. L.; Bursten, B. E. *Inorg. Chem.* **2005**, *44*, 2255. (b) Páez-Hernández, D.; Ramírez-Tagle, R.; Codorniu-Hernández, E.; Montero-Cabrera, L. A.; Arratia-Pérez, R. *Polyhedron* **2010**, *29*, 975. (c) Neidig, M. L.; Clark, D. L.; Martin, R. L. *Coord. Chem. Rev.* **2013**, *257*, 394.
(44) Mayer, I. *Chem. Phys. Lett.* **1983**, *7*, 270.
(45) (a) Nalewajski, R. F.; Mrozek, J. *Int. J. Quantum Chem.* **1994**, *51*, 187. (b) Nalewajski, R. F.; Mrozek, J.; Michalak, A. *Int. J. Quantum Chem.* **1997**, *61*, 589.
(46) (a) Michalak, A.; De Kock, R. L.; Ziegler, T. *J. Phys. Chem. A* **2008**, *112*, 7256. (b) Curley, J. J.; Piro, N. A.; Cummins, C. C. *Inorg. Chem.* **2009**, *48*, 9599. (c) Mills, D. P.; Cooper, O. J.; Tuna, F.; McInnes, E. J. L.; Davies, E. S.; McMaster, J.; Moro, F.; Lewis, W.; Blake, A. J.; Liddle, S. T. *J. Am. Chem. Soc.* **2012**, *134*, 10047. (d) Patel, D.; McMaster, J.; Lewis, W.; Blake, A. J.; Liddle, S. T. *Nat. Commun.* **2013**, *4*, 2323. (e) King, D. M.; Tuna, F.; McInnes, E. J. L.; McMaster, J.; Lewis, W.; Blake, A. J.; Liddle, S. T. *Nat. Chem.* **2013**, *5*, 482.
(47) (a) Reed, A. E.; Curtiss, L. A.; Weinhold, F. *Chem. Rev.* **1988**, *88*, 899. (b) Bader, R. F. W. *Atoms in Molecules: A Quantum Theory*; OUP: Oxford, U.K., 1990. (c) Mulliken, R. S. *J. Chem. Phys.* **1955**, *23*, 1833. (d) Mountain, A. R. E.; Kaltsoyannis, N. *Dalton Trans.* **2013**, *42*, 13477. (e) Jones, M. B.; Gaunt, A. J.; Gordon, J. C.; Kaltsoyannis, N.; Neu, M. P.; Scott, B. L. *Chem. Sci.* **2013**, *4*, 1189. (f) Schnaars, D. D.; Gaunt, A. J.; Hayton, T. W.; Jones, M. B.; Kirker, I.; Kaltsoyannis, N.; May, I.; Reilly, S. D.; Scott, B. L.; Wu, G. *Inorg. Chem.* **2012**, *51*, 8557. (g) Vlaisavljevich, B.; Miro, P.; Cramer, C. J.; Gagliardi, L.; Infante, I.; Liddle, S. T. *Chem.—Eur. J.* **2011**, *17*, 8424. (h) Arnold, P. L.; Turner, Z. R.; Kaltsoyannis, N.; Pelekanaki, P.; Bellabarba, R. M.; Tooze, R. P. *Chem.—Eur. J.* **2010**, *16*, 9623. (i) Petit, L.; Adamo, C.; Maldivi, P. *Inorg. Chem.* **2006**, *45*, 8517. (j) Manna, D.; Mula, S.; Bhattacharyy, A.; Chattopadhyay, S.; Ghanty, T. K. *Dalton Trans.* **2015**, *44*, 1332. (k) Rodríguez, J. I.; Köster, A. M.; Ayers, P. W.; Santos-Valle, A.; Vela, A.; Merino, G. *J. Comput. Chem.* **2009**, *30*, 1082. (l) Rodríguez, J. I.; Bader, R. F. W.; Ayers, P. W.; Michel, C.; Götz, A. W.; Bo, C. *Chem. Phys. Lett.* **2009**, *472*, 149.
(48) Rayón, V. M.; Redondo, P.; Valdés, H.; Barrientos, C.; Largo, A. *J. Phys. Chem. A* **2007**, *111*, 6334.
(49) Rayón, V. M.; Redondo, P.; Valdés, H.; Barrientos, C.; Largo, A. *J. Chem. Phys.* **2009**, *131*, 094507.
(50) (a) Andersen, R. A. *Inorg. Chem.* **1979**, *18*, 1507. (b) Monreal, M. J.; Thomson, R. K.; Cantat, T.; Travia, N. E.; Scott, B. L.; Kiplinger, J. L. *Organometallics* **2011**, *30*, 2031.
(51) Hooft, R. W. W. *COLLECT*; Nonius BV: Delft, The Netherlands, 1998.
(52) Otwinowski, Z.; Minor, W. *Methods Enzymol.* **1997**, *276*, 307.
(53) Sheldrick, G. M. *Acta Crystallogr., Sect. A* **2008**, *64*, 112.
(54) Farrugia, L. J. *J. Appl. Crystallogr.* **1997**, *30*, 565.

DOI: 10.1021/acs.inorgchem.5b00034
Inorg. Chem. 2015, 54, 2474−2490